Stratigraphic and structural reappraisal of the metamorphic complex of NE Cordillera Darwin, Tierra del Fuego, Chile

Pablo J. TORRES CARBONELL[1], Sebastián J. CAO[2], Fernando A. POBLETE[3], Marc POUJOL[4]

[1] Corresponding author. Centro Austral de Investigaciones Científicas (CADIC), CONICET, Ushuaia, Argentina, poltorrescarbonell@gmail.com, +54 2901 422310

[2] Instituto de Ciencias Polares, Ambiente y Recursos Naturales, Universidad de Tierra del Fuego, Ushuaia, Argentina, sebacao@gmail.com

[3] Departamento de Geología, Facultad de Ciencias Físicas y Matemáticas, Universidad de Chile, Santiago, Chile, ferpoble@uchile.cl

[4] Univ. Rennes, CNRS, Géosciences Rennes, UMR6118, F-35000 Rennes, France, marc.poujol@univ-rennes.fr

ABSTRACT. New petrographic and structural studies in NE Cordillera Darwin have impacts on the stratigraphic distinction between basement and cover of the Rocas Verdes Basin. Our results reveal that metasedimentary and metavolcanic rocks mapped in the hanging wall and footwall of the first-order Glaciar Marinelli Thrust were affected by the same episodes of Meso-Cenozoic deformation as the cover rocks of the Fuegian Andes, with no evidence of pre-Jurassic deformation. The key to determining the deformation sequence relies on correct interpretation of the primary sedimentary layering in fine-grained metasedimentary rocks. Our results suggest that the rocks in the study area are part of the sedimentary and volcanic fill of the Rocas Verdes Basin. Two new U-Pb age determinations indicate that early Paleozoic and older detrital zircon grains prevail in these cover rocks, consistent with provenance from an eroded Paleozoic basement during the early development of the rift basin. Careful petrographic studies are required to assess the validity of detrital zircon maximum depositional ages in the area.

Keywords: Structural geology, Stratigraphy, Metasedimentary cover, Rocas Verdes Basin, Fuegian Andes, Cordillera Darwin

Reevaluación estratigráfica y estructural del complejo metamórfico del noreste de Cordillera Darwin, Tierra del Fuego, Chile. Nuevos estudios petrográficos y estructurales en el noreste de Cordillera Darwin nos permiten distinguir estratigráficamente entre el basamento y la cobertura de la Cuenca Rocas Verdes. Estos resultados muestran que las rocas metasedimentarias y metavolcánicas mapeadas en los bloques yacente y colgante del corrimiento Glaciar Marinelli fueron afectadas por los mismos episodios de deformación meso-cenozoica que las rocas en la cobertura de los Andes Fueguinos, sin evidencias de

deformación pre-jurásica. La clave para definir la secuencia de deformación está en la correcta distinción de la laminación primaria en las rocas metasedimentarias de grano fino. Los resultados sugieren que las rocas estudiadas son parte del relleno sedimentario y volcánico de la Cuenca Rocas Verdes. Dos nuevas dataciones por U-Pb indican que en estas rocas predominan circones detríticos del Paleozoico temprano o más antiguos, lo cual es consistente con la proveniencia desde un basamento paleozoico erosionado durante el desarrollo temprano del rift. La validez de las edades máximas de sedimentación a partir de dataciones en circones detríticos en el área debe ser evaluada mediante estudios petrográficos de detalle.
Palabras clave: Geología estructural, Estratigrafía, Cobertura metasedimentaria, Cuenca Rocas Verdes, Andes Fueguinos, Cordillera Darwin

1. Introduction

Stratigraphic interpretation of metasedimentary facies in the Fuegian Andes is a problematic issue that geologists have had to confront since the earliest geological studies in this region. In some areas the degree of deformation is such that separation between stratigraphic units based exclusively on lithology is not possible. In recent years, geochronological determinations allowed distinction between units with very similar lithologies (e.g., phyllites or slates). Although helping to separate Cretaceous and Jurassic units with synsedimentary tuffaceous components, this approach has limitations when dealing with sedimentary facies that were not contemporary with volcanism.

Determining the stratigraphic order of mostly fine-grained metasedimentary rocks of the Paleozoic basement and Mesozoic sedimentary cover in the Fuegian

Andes is especially challenging. The facies similarity between some horizons in these rock units has been recognized since the early investigations in Cordillera Darwin (Kranck, 1932; Fester, 1938). Strong deformation and regional metamorphism during the Late Cretaceous largely obliterated original stratigraphic relationships, hampering distinction in the field (Kranck, 1932; Johnson, 1990; Hervé *et al.*, 2010a). In addition, the scarcity of zircon coeval with sedimentation in the protoliths usually rules out geochronological distinction, a problem that extends beyond the local area of the Fuegian Andes (Hervé *et al.*, 2010a; Cawood *et al.*, 2012; Rossignol *et al.*, 2019; Copeland, 2020; Cao *et al.*, 2022; Castillo *et al.*, 2022).

Here we report a detailed revision of the rocks exposed in NE Cordillera Darwin, a region with contrasting stratigraphic interpretations of the basement and cover units. We consider that detailed petrographic analysis, together with the identification of structural generations from macroscopic and microstructural studies, is key to separating basement from cover. Mineral dating (e.g., detrital zircon U-Pb ages), however, may be of limited value when the objective is to determine the true stratigraphic position of these rocks, which rarely had coeval volcanism. Our updated review, based on new mapping, petrographic and microstructural analyses, allows us to improve the geological map accuracy of this area and organize the stratigraphic and structural framework, with the aims of unifying criteria and facilitating future research in such a complex terrane.

2. Geological setting

2.1. Deformation events and metamorphism in the central belt of the Fuegian Andes

Cordillera Darwin is the structural culmination of the Fuegian Andes. It exposes Paleozoic basement of the southwestern margin of Gondwana and overlying Mesozoic cover rocks exhibiting intense Cretaceous and Cenozoic deformation. The cover rocks were deposited in a Jurassic volcano-tectonic rift basin that evolved into a back-arc basin (Rocas Verdes Basin), with active marine sedimentation lasting until the end of the Early Cretaceous (Katz, 1963; Dalziel *et al.*, 1974; Suárez and Pettigrew, 1976; Wilson, 1991; Olivero and Martinioni, 2001). These rocks, whose stratigraphic framework is described below, were affected by two main episodes of deformation, associated with the Late Cretaceous closure of the basin and the Cenozoic formation of a retro-arc thrust-fold belt, respectively. Closure of the Rocas Verdes Basin involved north-northeastward obduction of the basin floor and south-southwestward underthrusting of its continental margin, followed by collision of this margin with the subduction-related magmatic arc (Nelson *et al.*, 1980; Dalziel, 1986; Cunningham, 1995; Klepeis *et al.*, 2010). The evolution of the thrust-fold belt included the development of duplex thrust systems and transference of shortening towards the retro-arc foreland basin, leading to exhumation of the internal orogen in the central belt (Álvarez-Marrón *et al.*, 1993; Rojas and Mpodozis, 2006; Klepeis *et al.*, 2010; Torres Carbonell *et al.*, 2020; Cao *et al.*, 2023).

The central belt of the Fuegian Andes (Fig. 1) thus involves rocks deformed by two main events. These are briefly introduced here, while a more detailed

description of structures pertaining to our study area is given in section 2.3. The first generation of structures, caused by the closure of the Rocas Verdes Basin, involved intense deformation associated with the development of ductile shear zones and thrusts during obduction and underthrusting (Fig. 1). This deformation was coeval with regional metamorphism, with the higher grades (upper amphibolite facies) attained by the basin fill and its basement at mid-crustal levels between 90 and 70 Ma (Cunningham, 1994, 1995; Kohn *et al.*, 1995; Klepeis *et al.*, 2010; Maloney *et al.*, 2011). The lower metamorphic grades are shown by phyllites and slates of the uppermost structural levels, comprising the metamorphosed Cretaceous sedimentary cover of the Rocas Verdes Basin and the foreland basin initiated during this orogenesis. These rocks suffered varying intensities of ductile deformation (Bruhn, 1979; Nelson *et al.*, 1980; Torres Carbonell *et al.*, 2017), which in the central belt was labelled $D1_{CB}$ by Torres Carbonell *et al.* (2020; CB: central belt, Fig. 1).

The second generation of structures recognized in the central belt includes mostly brittle-ductile and brittle faults, which comprise the roots of the Fuegian thrust-fold belt (Klepeis, 1994; Rojas and Mpodozis, 2006; Torres Carbonell *et al.*, 2020; Cao *et al.*, 2023). These thrust faults are interpreted as responsible for exhumation of the mid-crustal rocks exposed in the central belt, i.e., the higher-grade metamorphic rocks juxtaposed with the shallower cover rocks of the Rocas Verdes Basin. In the more deformed rocks, the thrusts formed simultaneously with some ductile deformation, such as development of a crenulation cleavage, often localized near the fault zones and sparser or absent towards the foreland (Cao *et al.*, 2023). Thrust stacking in the central belt enables the study of different structural levels of the earlier $D1_{CB}$ deformation. The development of the thrust-fold belt and related structures was labelled $D2_{CB}$ (Torres Carbonell *et al.*, 2020; Fig. 1).

2.2. Central belt stratigraphy

2.2.1. Historical perspective

The currently accepted stratigraphic framework of Cordillera Darwin is the result of almost 100 years of geological investigation. In Table 1 we provide a synthesis of the stratigraphic nomenclature of the main units addressed here and its modifications in successive studies, which helps to correlate stratigraphic names through time. We restrict our analysis to the northern flank of Cordillera Darwin, where low-grade metamorphic rocks crop out. The higher-grade rocks, cropping out in fjords on the southern flank, include a complex tectonized mixture of several units (cf. Klepeis *et al*., 2010), whose analysis is beyond the objective of this work.

The first detailed petrological study of Cordillera Darwin was published by E. Kranck in 1932. His initial rough stratigraphic separation distinguished: 1) "*high metamorphic, micaceous and quartzitic schists of the Darwin Cordillera and its westerly and easterly continuation*", and 2) "*argillitic and phtanitic schists of the Beagle regions and north front of the Central Cordillera (Mount Buckland and Yahgan Formations)*" (pp. 25–26). The first unit is distributed in what the author called the "central core of the High Cordillera", which occupies the area between Ushuaia and Península Brunswick (Fig. 1), and consists of "*strongly tectonized and recrystallized schists*" and abundant "*altered greenstones*", metamorphosed into chlorite- and talc-schists. The second unit (Monte Buckland and Yahgan formations) is now included in the Tobífera Formation-Lemaire Complex and the Yahgan Formation, which are described in the next section.

Although Kranck (1932) is frequently cited for recognizing the "unconformity" between the metamorphic basement of Cordillera Darwin and its cover, this surface

168 is not actually exposed and was interpreted on the basis of the stratigraphic
169 relationships exposed in northern Fiordo De Agostini (Monte Buckland section). In
170 that section he described fine micaceous schists with muscovite and biotite, above
171 which there are several levels of conglomerate-agglomerate with clasts of schists
172 and quartzose matrix. These conglomerates are interlayered with quartz-porphyry
173 schists (the Tobífera Formation), which are in turn covered by slates and tuffs.
174 Regarding the contact with the basal fine micaceous schists, Kranck (1932) stated
175 that due to the strong deformation, it "*is as yet difficult to decide if the contact in*
176 *question is a primary one, if there is a disconformity between the old schist of the*
177 *Central-Cordillera and the quartz-porphyry formation, or if the contact is a tectonical*
178 *one*" (p. 63). The strongest argument pointing towards an unconformity is the
179 presence of conglomerates with clasts of schists, but the unconformity itself is not
180 exposed.

181 Observations in Fiordo Relander and especially in Fiordo Finlandia led Kranck
182 (1932) to conclude that the quartz-porphyry schists "*also occur in the inner parts of*
183 *the Central-Cordillera in strongly metamorphic condition, and that it therefore is*
184 *hardly possible to separate the old central schists (older than Monte Buckland*
185 *Formation) and the fossil-bearing slates of the Monte Buckland series in these parts*
186 *of the mountain range*" (p. 81). In summary, Kranck (1932) proposed an
187 unconformity between the Tobífera Formation ("quartz porphyry schists" or Monte
188 Buckland Formation) and the "high metamorphic schists", "central schists" or "old
189 schists" of Cordillera Darwin, despite acknowledging that the contact between the
190 two units was not clearly exposed, and that they were tectonically interleaved (pp.
191 114, 203–204).

192 It should be noted that even though he referred to the older unit as “high
193 metamorphic schists”, Kranck (1932) described no high-grade parageneses.
194 Overall, the author assigned a greenschist facies to all these schists (*ibid.*, pp 147–
195 148).

196 In our study area, based on samples collected by P. Quensel in 1908, Kranck
197 (1932) interpreted the same “highly metamorphic schists” described in the Central
198 Cordillera (Kranck, 1932, p. 88). To the south, in the head of Lago Acigami (Roca),
199 he mapped “schists of Lapataia” (pp. 93–95), which include metasedimentary rocks
200 and greenschists of basic igneous protolith, interlayered with coarse conglomerate
201 with clasts of deformed quartzitic schist, similar to conglomerates within the Tobifera
202 Formation (Monte Buckland series) above the interpreted unconformity in the Monte
203 Buckland section.

204 Much later, the work by Nelson *et al.* (1980) condensed the stratigraphic
205 results of the few published and several unpublished studies in the region at that
206 time. It also supported the existence in northern Cordillera Darwin of an unconformity
207 between the “basement complex” and a “cover complex”. Although their descriptions
208 are not detailed, they maintained the characterization of the basement complex
209 made by Kranck (1932) as essentially metapelitic rocks with minor amounts of
210 quartzite and greenstone (basic metavolcanic rock). Nelson *et al.* (1980) also
211 established a generalized cover succession that begins with a basal conglomerate
212 with clasts of volcanic and basement rocks, the latter with inherited deformation
213 fabrics. A silicic volcanic sequence with interlayered sedimentary horizons overlies
214 this basal unit and is covered by volcaniclastic sedimentary rocks.

215 Johnson (1990) gave more detailed descriptions of the basal conglomeratic
216 rocks, which he called “Basal Clastic Complex”. This unit covers the basement with

217 an inferred angular unconformity, or even by fault contact at some places. The
218 coarse facies include clasts of phyllites and schists derived from the basement.
219 Pyroclastic beds that form the base of the Seno Almirantazgo Volcanic-Sedimentary
220 Complex conformably cover the Basal Clastic Complex, which is not evenly
221 distributed since at some localities the tuffaceous deposits rest directly over the
222 basement (without an exposed contact). More recent work included the Basal Clastic
223 Complex and the Seno Almirantazgo Complex in the Tobífera Formation (Ortiz,
224 2007; Hervé *et al.*, 2010a). Johnson (1990) interpreted the semi-chaotic deposits of
225 low textural and mineralogical maturity of the Basal Clastic Complex as rift deposits
226 (avalanches), which incorporated eroded basement and clasts of the first volcanic
227 products of the Rocas Verdes Basin. Descriptions of the basement unit made by
228 Johnson (1990) are similar to those of Kranck (1932), emphasizing the
229 metapsammitic protoliths of the schists and phyllites, and their greenschist facies
230 metamorphic grade.

231 The only stratigraphic work in our study area, between Lago Fagnano and
232 south of Paso de las Lagunas, is that of Klepeis (1994), discussed in more detail
233 below. He recognized a major thrust fault (the “basement thrust”), which was thought
234 to place “Paleozoic-Mesozoic basement schists” over the Lower Cretaceous La
235 Paciencia Formation. Within the basement schists, Klepeis (1994) distinguished a
236 felsic or siliceous facies, possibly metatuffs and meta-agglomerates, interlayered
237 with more pelitic lithologies.

238 Later detailed analyses of the metamorphism in northern Cordillera Darwin
239 confirmed no difference in metamorphic grade between the units mapped as
240 basement and cover, ascribing the highest metamorphic grade to the Late
241 Cretaceous orogeny (Kohn *et al.*, 1993; Ortiz, 2007). These works revealed that in

242 the northern flank of Cordillera Darwin, greenschist facies index minerals are chlorite
243 and biotite, with garnet restricted to the internal region. It was suggested that the
244 basement unit was deformed before deposition of cover rocks, as indicated by the
245 occurrence of deformed metamorphic rock fragments in the Basal Clastic Complex.
246 This old deformation was attributed to early Mesozoic regional deformation in the
247 margin of Gondwana (cf. Dalziel and Elliott, 1971), with two published Jurassic zircon
248 U-Pb ages in granitic dikes cutting a prior foliation, constraining it as pre-Andean
249 (Klepeis *et al.*, 2010; Hervé *et al.*, 2010a).

250 Recent research employing detailed petrographic descriptions,
251 thermobarometric estimations and, more importantly, isotopic age determinations,
252 has corroborated most of the descriptions of the basement and cover units. The most
253 relevant stratigraphic update from this research is the definition of the Cordillera
254 Darwin Metamorphic Complex, which includes both pre-Jurassic basement and
255 Mesozoic cover rocks (Hervé *et al.*, 2010a).

256 It is important to recognize that the metasedimentary nature of both the
257 basement and part of the cover hampers distinction between them in different maps
258 (cf. Johnson, 1990; Ortiz, 2007; Hervé *et al.*, 2010a). The distinction is not always
259 resolved by geochronological studies: Hervé *et al.* (2010a) found that rocks mapped
260 as the Rocas Verdes Basin cover have prominent Paleozoic or older detrital zircon
261 age peaks, while only a few grains (frequently less than 10) have Jurassic ages. This
262 indicates a dominant detrital input from the basement, even within the volcanic-
263 sedimentary complex of the Tobífera Formation, as shown elsewhere in the basin
264 (Calderón *et al.*, 2007). This idea was recently used in redefinition of the age of the
265 Lapataia Formation by Cao *et al.* (2022), which we address in more detail below.

Recently, Mella and Quiroz (2023) studied the Svea granite (Quensel, 1910) for which they reported a Late Devonian $^{40}Ar/^{39}Ar$ muscovite age, as well as an early Carboniferous $^{40}Ar/^{39}Ar$ muscovite age for an orthogneiss interpreted as a contact metamorphic product. They identified an unconformable cover to the Svea granite of quartzites and metaconglomerates, which they named “Estratos Paso de las Lagunas”, previously mapped as the Lower Cretaceous La Paciencia Formation by Klepeis (1994).

2.2.2. Stratigraphic synthesis

We now briefly describe an updated stratigraphic framework of the northern flank of Cordillera Darwin. Notice that various units from the pre-Jurassic basement to the Lower Cretaceous rocks were incorporated into the Cordillera Darwin Metamorphic Complex by Hervé *et al.* (2010a), as already mentioned. We describe them separately here.

Pre-Jurassic basement

This unit is composed of metasedimentary rocks and granitic intrusions. The metasedimentary components include phyllites and fine schists, with quartz, muscovite, biotite, chlorite, and epidote. They are derived from fine-grained sedimentary rocks. A subordinate facies of greenstones or greenschists, with more abundant chlorite, epidote and amphibole, is possibly derived from basic igneous rocks (Kranck, 1932). The metamorphic grade of these rocks is within the greenschist facies, mostly within the chlorite and biotite isograds. Only at the heads of Fiordo Brookes and Fiordo Parry are these rocks within the garnet isograd, close to granitic intrusions and along with the higher-grade metamorphic zone of Cordillera

Darwin (Kranck, 1932; Kohn *et al.*, 1993; Kohn *et al.*, 1995; Ortiz, 2007). The mostly buried contact with the Rocas Verdes Basin cover is an interpreted unconformity that has never been described precisely.

Granitic intrusions of the basement include the Devonian Svea granite, overprinted by an episode of early Carboniferous metamorphism (Mella and Quiroz, 2023). This rock is unconformably covered by the Estratos Paso de las Lagunas (see above). No other granite of Paleozoic age is known from the study area. However, recent findings in Argentina indicate the presence of exhumed Paleozoic granitic basement in the horsts of Jurassic hemigrabens, unconformably covered by sedimentary and tuffaceous facies of the Lemaire Complex (Lobo *et al.*, 2024). Also, Paleozoic granites have been cored in the subsurface of the Austral-Magallanes basin in northern Tierra del Fuego (Söllner *et al.*, 2000; Hervé *et al.*, 2010b; Castillo *et al.*, 2017; de la Cal *et al.*, 2023).

Hervé *et al.* (2010a) provided several detrital zircon U-Pb ages from schists of the Cordillera Darwin Metamorphic Complex that may be considered part of the pre-Jurassic basement, especially (according to those authors) samples with Carboniferous youngest zircon ages, and Devonian, Ordovician, Cambrian and older age peaks. We will discuss these results in more detail in this work.

Lapataia Formation. Jurassic

The Lapataia Formation has its type area at the southwestern corner of Argentine Tierra del Fuego, cropping out in a ~10 km wide belt east of the international boundary. It extends into Chilean territory along the head of Lago Acigami; according to Kranck (1932), similar rocks are exposed between this lake

315 and Paso de las Lagunas. In the type area the Lapataia Formation is thrust onto the
316 Lemaire Complex, and its base and thickness are unknown.

317 The Lapataia Formation consists of a metasedimentary facies of phyllites
318 and very fine schists with quartz, muscovite, chlorite and minor biotite, and a
319 metabasic facies formed by greenschists and greenstones (Cao *et al.*, 2018, 2022).
320 The metasedimentary facies reveals primary sedimentary layering, formed by an
321 alternation of quartzite layers and metapelitic layers with muscovite, chlorite and
322 occasional biotite porphyroblasts. The sedimentary layering is transposed by the
323 dominant tectonic foliation, formed during $D1_{CB}$ (Cao *et al.*, 2018; Torres Carbonell
324 *et al.*, 2020). The metabasites represent a basic volcanic or pyroclastic protolith, and
325 are distinguished by abundant epidote and tremolite-actinolite.

326 Four samples from the coarsest horizons of the metasedimentary facies
327 gave several Paleozoic detrital zircon U-Pb ages, with none younger than Permian
328 (Cao *et al.*, 2022). A thorough structural and petrographic examination of the rock
329 showed no tectonic deformation older than Late Cretaceous $D1_{CB}$, but revealed
330 clasts of foliated metamorphic rocks with an inherited deformation, which led Cao *et*
331 *al.* (2018, 2022) to interpret this unit as part of the cover of the Rocas Verdes Basin
332 with a possible Jurassic age. It therefore represents the deposits of the early rifting
333 during opening of the basin, with abundant detritus supplied from eroded basement
334 highs. Cao *et al.* (2022) concurred with Hervé *et al.* (2010a) in considering that the
335 absence of Jurassic zircons cannot be solely used to assess the depositional age of
336 these rocks, especially when they lack coeval volcanic material. We will further
337 discuss this aspect in section 5.2.

338

339 ***Tobífera Formation-Lemaire Complex. Middle Jurassic-Berriasian***

The Tobífera Formation was defined from subsurface data in northern Tierra del Fuego and includes exposures of mainly silicic volcanic and associated rocks along the southern Patagonian and Fuegian Andes (Thomas, 1949). Studies in Tierra del Fuego recognized acidic and less abundant basic volcanic rocks, several pyroclastic facies, and associated volcaniclastic and marine sedimentary deposits, accumulated during the rifting that affected this portion of Gondwana in the Jurassic (Cortés and Valenzuela, 1960; Dalziel *et al.*, 1974; Bruhn *et al.*, 1978; Johnson, 1990; Hanson and Wilson, 1991; González Guillot *et al.*, 2016; Cao *et al.*, 2022). This unit is more easily recognized in outcrops when it consists of felsic porphyries (cf. Kranck, 1932), but generates confusion when represented by metasedimentary facies, especially in highly deformed zones where these rocks are interlayered with the supposed basement schists (e.g., at Fiordo Relander and Fiordo Finlandia; cf. Kranck, 1932; Ortiz, 2007). The inclusion of the Basal Clastic Complex of Johnson (1990) as an integral part of the Tobífera Formation (cf. Ortiz, 2007; Hervé *et al.*, 2010a) adds a variety of clastic facies to this volcano-sedimentary complex, with an importance within the sequence that is usually minimized. In fact, this coarse-grained succession is usually ascribed to the base of the formation mainly due to description of isolated outcrops in the Monte Buckland section, and at Fiordo Brookes, Bahía Ainsworth, and Fiordo Parry. However, there are also similar coarse-grained horizons at intermediate positions within the Tobífera Formation (Johnson, 1990), including the succession distinguished by Cortés and Valenzuela (1960) as the Río Fontaine Formation in the eponymous river (see Table 1). Also, several conglomerate and sandstone horizons and lenses are known from the equivalent Lemaire Complex in Argentina (see Cao *et al.*, 2025 for a review).

364 The age of the Tobífera Formation-Lemaire Complex is constrained from
365 dating of the volcanic and volcaniclastic horizons with U-Pb zircon ages that range
366 from Middle Jurassic to Berriasian (Calderón *et al.*, 2007; Hervé *et al.*, 2010a; Palotti
367 *et al.*, 2012; Cao *et al.*, 2025). These ages, however, are restricted to facies with a
368 prominent acidic volcanic composition, such as rhyolites and ignimbrites. In other
369 horizons where a tuffaceous composition is not dominant, recycled Paleozoic detrital
370 zircons are more abundant. For example, Hervé *et al.* (2010a) reported detrital zircon
371 U-Pb ages from samples within the Tobífera Formation sedimentary horizons in
372 Cordillera Darwin. One sample (FO0524) gave Early Triassic ages and a prominent
373 Cambrian age peak, but no Jurassic ages. Another sample (FO0539) gave a
374 prominent Carboniferous age peak and only two grains (three SHRIMP spots) with
375 Middle Jurassic ages. Finally, a granodiorite clast near the base of the Tobífera
376 Formation at Fiordo Parry (sample FO0516) has an Ordovician crystallization age.
377 More significantly, sample FO0508, mapped as basement in an amphibolitic schist
378 with garnet and biotite, has a prominent Devonian age peak but six grains (eight
379 spots) record Middle Jurassic ages. Otherwise, in the absence of Jurassic grains,
380 Hervé *et al.* (2010a) proposed as a working hypothesis that samples with Permian
381 or Triassic ages could be considered part of the cover. However, samples that
382 possibly belong to the cover also have older detrital zircon ages. This highlights the
383 problem studied by Cao *et al.* (2022) in the Lapataia Formation, mentioned above,
384 which applies similarly to the Tobífera Formation. Below, we will compare in detail
385 some of the samples mentioned here with our data.

386 Granites of the Darwin suite exposed in southern Cordillera Darwin have
387 been associated genetically with the Tobífera Formation (Hervé *et al.*, 1981). These

have U-Pb zircon crystallization ages between Middle and Late Jurassic (Mukasa and Dalziel, 1996; Klepeis *et al.*, 2010).

Río Jackson and La Paciencia Formations. Lower Cretaceous

Slates and shales of the La Paciencia Formation crop out in the northern flank of Cordillera Darwin at Fiordo Brookes and Bahía Ainsworth, where the contact with the older Tobífera Formation is tectonic. The La Paciencia Formation was defined north of Lago Fagnano, where it contains Cretaceous fossils (Cortés and Valenzuela, 1960). Towards the east, in Argentina, it corresponds to the Beauvoir Formation, with Aptian-Albian invertebrates and consistent U-Pb detrital zircon ages near its base (Olivero *et al.*, 2009; Martinioni *et al.*, 2013; Cao *et al.*, 2025). These mostly fine-grained sedimentary and metasedimentary rocks contain abundant thin intercalations of tuffaceous horizons, usually a few centimetres thick. North of Lago Fagnano, the La Paciencia Formation conformably rests on a relatively thin horizon (less than 100 m thick) of intercalated shales, marls, and fossiliferous limestone, known as the Río Jackson Formation (Cortés and Valenzuela, 1960). This latter formation lies over the Tobífera Formation with a tectonic contact (thrust detachment; Klepeis, 1994).

Klepeis (1994) mapped the Río Jackson and La Paciencia formations south of Lago Fagnano, in a NW-SE belt between Cerro Verde and Cerro Svea. Some of these rocks were included in the previously mentioned Estratos Paso de las Lagunas by Mella and Quiroz (2023). These rocks are one of the main topics of study in this work, and will be addressed below.

Late Cretaceous Beagle Suite

413 The youngest intrusive rocks cropping out in northern Cordillera Darwin
414 comprise some diorite stocks and dikes affecting the Cerro Matrero Formation in the
415 northern area of Fiordo Brookes (Johnson, 1990), and granitic intrusives mapped at
416 Fiordo Parry and south of Cerro Svea (Nelson *et al.*, 1980; Johnson, 1990; Hervé *et*
417 *al.*, 2010a; Klepeis *et al.*, 2010). Both the Darwin and Beagle suites crop out in the
418 inner portion of Fiordo Parry (Nelson *et al.*, 1980; Ortiz, 2007; Hervé *et al.*, 2010a;
419 Klepeis *et al.*, 2010). Klepeis (1994) mapped a possible granite south of Cerro Svea,
420 which has not been studied in detail.
421

422 **2.3. Previous structural work**

423 Several previous studies highlighted the structural complexity of Cordillera
424 Darwin (Nelson *et al.*, 1980; Dalziel and Brown, 1989; Klepeis, 1994; Klepeis *et al.*,
425 2010; Betka *et al.*, 2022). We will restrict our analysis of previous research to the
426 area directly relevant to our work, in northern Cordillera Darwin, which includes the
427 work of Nelson *et al.* (1980) and Klepeis (1994). Similar work directly east of this
428 area, in Argentina, was performed by Bruhn (1979) and later by Cao *et al.* (2018,
429 2023). A comparison of the generations of regionally recognized structures is given
430 in Table 2, while the regional tectonic context is discussed by Torres Carbonell *et al.*
431 (2020) and Cao *et al.* (2023).

432 Nelson *et al.* (1980) established a regional deformation sequence that starts
433 with a pre-Jurassic deformation of the basement (Db; see Table 2), which was not
434 clearly distinguished from younger structures, was not illustrated in detail, and seems
435 to be inferred from the occurrence of foliated rock fragments in conglomerates of the
436 Tobífera Formation. The first “Andean” deformation distinguished by Nelson *et al.*

(1980) is a “strongly developed foliation” that is more intense in southern Cordillera Darwin. In northern Cordillera Darwin (but west of our study area), this deformation is a slaty cleavage at high angles to bedding and axial-planar to open folds. In the basement unit (it is not clear if this refers to northern or southern areas) it is a phyllitic or schistose foliation in pelitic lithologies, axial-planar to tight or isoclinal folds in siliceous rocks. This foliation, called S1 by Nelson *et al.* (1980), has associated stretching and intersection lineations called L1.

The subsequent structural generation described by Nelson *et al.* (1980) differs between the northern and southern areas of Cordillera Darwin. To the south, it is a complex set of macroscopic and mesoscopic folds and axial-planar cleavage (S2), which fold previous S1 surfaces and were formed during peak metamorphic conditions. Metamorphic porphyroblasts such as staurolite and large amphiboles grew coevally with the S2 foliation. However, in our area of interest in northern Cordillera Darwin, Nelson *et al.* (1980) described S2 as an anastomosed phyllitic cleavage that intersects S1 at low angle, in a way “*similar to shear fracture cleavages (SF-tectonite fabrics)*” (p. 738). We emphasize that these terms (fracture cleavage, SF-tectonite) are now anachronistic, but refer to spaced foliations, and possibly foliated cataclasites. The spaced foliation associated with brittle or brittle-ductile structures is clearly different from the S2 cleavages formed during the staurolite-grade metamorphism in southern Cordillera Darwin. The spaced S2 foliation described by Nelson *et al.* (1980) in northern Cordillera Darwin is the youngest structure that they recognized in this area, since their D3 deformation is restricted to southwestern Cordillera Darwin.

The work of Nelson *et al.* (1980) constituted the cornerstone for subsequent structural work in the region, including the detailed mapping by Klepeis (1994), who

462 interpreted a NW-SE belt of Lower Cretaceous rocks (Río Jackson and La Paciencia
463 formations) between Cerro Verde and south of Paso de las Lagunas (see Klepeis'
464 original map in Supplementary File 1). The southern boundary of this belt is a thrust,
465 interpreted as carrying the Paleozoic basement over the Lower Cretaceous rocks
466 ("basement thrust" in Klepeis, 1994). In a more recent work this has been called the
467 Glaciar Marinelli Thrust (Rojas and Mpodozis, 2006).

468 Klepeis (1994) described structures above and below this major thrust, using
469 labelling that cannot be directly correlated across it (e.g. S1 in the hanging wall is
470 older and different from S1 in the footwall). In the footwall, Klepeis (1994) described
471 the structures shown in Table 2. The "dominant foliation" (S1) is a penetrative, finely
472 spaced cleavage defined by aligned muscovite and chlorite and anastomosed
473 pressure-solution seams, with flattened feldspars and dynamically recrystallized
474 quartz in the microlithons. This foliation cuts the recognized sedimentary lamination
475 (S0) at a low angle. A penetrative downdip mineral lineation (L1) is distinguished on
476 S1 surfaces and is formed by the preferred alignment of flattened porphyroclasts
477 and muscovite.

478 A second structure mentioned by Klepeis (1994) is a "*fine spaced cleavage*
479 *at low angle to S1*", which dips to the south or west, and is called S2. He gave no
480 further detail about this structure.

481 Finally, Klepeis (1994) described a "*moderately dipping crenulation cleavage*
482 *that deforms S1 and S2*", called S3. This structure is not as conspicuous as S1, with
483 its best development near the Glaciar Marinelli Thrust. Broad and open minor folds
484 (F4) are developed on earlier fabrics. Klepeis (1994) interpreted S1, L1, and S2 in
485 the footwall of the Glaciar Marinelli Thrust as equivalent to S1, L1, and S2 as
486 described by Nelson *et al*. (1980) in northern Cordillera Darwin (see Table 2).

In the hanging wall of the Glaciar Marinelli Thrust, Klepeis (1994) described "*an early foliation observed mainly in thin section*", also labelled S1. This foliation is defined by the preferred orientation of aligned muscovite and chlorite, quartz aggregates and pressure-solution seams. It is subparallel to quartz veins and is deformed into isoclinal folds together with them (F2).

According to Klepeis (1994), the "dominant" foliation in the Glaciar Marinelli Thrust hanging wall is "an intensely penetrative crenulation cleavage" that overprints S1, and is called S2 (Table 2). This cleavage is defined by pressure-solution seams and "new" chlorite and muscovite, and is axial-planar with the F2 folds. Remarkably, this S2 in the hanging wall is coplanar with the S1 in the footwall of the thrust. S2 has an associated downdip stretching lineation (L2), defined by stretched and recrystallized quartz porphyroclasts.

S2 in the hanging wall is crenulated by a third foliation enhanced by pressure-solution seams, called S3 by Klepeis (1994), with associated small, tight and upright folds (F3). This S3 crenulation is deformed by low-angle shear bands with gentle dips, both to the south and north. Broad, open folds in the previous foliations (F4) are associated with development of these shear bands, with usual top-to-northeast shear sense.

The overprinting relationships interpreted by Klepeis (1994) led him to correlate S1 in the hanging wall with the Db deformation of Nelson *et al.* (1980), and his "dominant foliation" S2 with the dominant fabric in basement rocks of Nelson *et al.* (1980), which they called S1 (see Table 2). Accordingly, S3 would correspond to S2 of Nelson *et al*. (1980).

3. Methods

Fieldwork in the study area (Fig. 2) was focused on mapping of lithologies and structures. We collected orientated samples for microstructural and petrographic studies on sites shown on the map. Samples CD05 and CD06 were collected for U-Pb dating of detrital zircons (locations given in Supplementary File 2). Sample CD05 is a metasedimentary phyllite in the hanging wall of the Glaciar Marinelli Thrust, a unit mapped as Paleozoic-Mesozoic basement by Klepeis (1994; see Supplementary File 1). Sample CD06 is a metapsammite intercalated with breccias and dark slates at Paso de las Lagunas, which was mapped by Klepeis (1994) as La Paciencia Formation (see Supplementary File 1), and by Mella and Quiroz (2023) as Estratos Paso de las Lagunas.

Both samples were analysed for geochronology at the GeOHeLiS platform, University of Rennes (France) by laser ablation inductively coupled plasma mass spectrometry (LA-ICP-MS). The detailed analytical methods are explained in Supplementary Files 3 and 4, and results are listed in Supplementary File 2. Only 90–110% concordant data were used. Single-grain concordia ages according to Vermeesch (2021a) were calculated using *IsoplotR* (Vermeesch, 2018); these were only used for the kernel density estimation (KDE) diagrams, all the rest of the ages mentioned in the text are apparent ages ($^{206}Pb/^{238}U$ when age <1000 Ma, else $^{207}Pb/^{206}Pb$) or calculations derived from them. The maximum depositional ages are reported as the weighted mean of the youngest three zircons with overlapping 2σ uncertainty (Y3Go), following the criteria suggested by Dickinson and Gehrels (2009), Coutts *et al.* (2019), Copeland (2020), and Sharman and Malkowski (2020). We also report the age of the youngest single grain (YSG) and the maximum

likelihood (MLA) method of Vermeesch (2021b). Single-grain concordia age and MLA errors are reported as 2σ, whilst for the Y3Go and YSG ages errors are 2se.

All structural and microstructural descriptions made here follow terminologies stated by Passchier and Trouw (2005) and Twiss and Moores (2007). For clarity in the comparison of structures defined by previous authors, we added letters to the labels that refer to structural generations, indicating the last name of the respective author (e.g., Table 2). We used *Stereonet* software from R.W. Allmendinger to plot equal-area spherical projections of structural data.

4. Results

4.1. Field geology and petrography

We describe in this section the lithological and structural relationships at both outcrop and microscopic scale, as observed in two areas (Fig. 2): 1) between the Glaciar Marinelli Thrust and the northern flank of Cerro Skottsberg (footwall of this thrust), and 2) the western flank of Cañadón del Horno (hanging wall).

4.1.1. Footwall of the Glaciar Marinelli Thrust

The rocks exposed here include intercalated rhyolite, chloritic fine-grained schists (tuffs), schistose breccias, metapsammites, and slates. The contacts between these facies are usually obliterated or very difficult to distinguish due to intense deformation. The rhyolite crops out at CD08 (Fig. 3A; see locations in figure 2), intercalated with chloritic schists with deformed or unexposed contacts, and develops a rough disjunctive foliation, which dips moderately to the SW (Fig. 2). Under the microscope (Fig. 3B), the rhyolite has porphyritic texture, with a fine-

559 grained felsitic groundmass revealing devitrification (spherulitic texture). Fine-
560 grained sericite is orientated, forming rough cleavage domains with variable spacing,
561 and microlithons with weakly orientated fabric. Pressure-solution seams also define
562 the cleavage domains. Phenocrysts are variably sized quartz, subhedral-to-euhedral
563 plagioclase and sanidine, and glomerocrysts formed by these three species.
564 Individual quartz crystals are anhedral or euhedral with perfect hexagonal habits, as
565 well as embayments and slight deformation features (lamellae, undulose extinction
566 and subgrain development). Accessory minerals include zircon, allanite and biotite,
567 completely replaced by pseudomorphic chlorite. Epidote and chlorite comprise the
568 main metamorphic minerals. The modal classification is a rhyodacite with 15% alkali-
569 feldspar, 41% plagioclase and 44% quartz.

570 The intercalated chloritic schists (Fig. 3C) have a conspicuous green
571 coloration in outcrop and are frequently cut by quartz veins. They have a very well-
572 developed cleavage and a stretching lineation in cleavage planes. Typical exposures
573 are those seen at CD07 and CD09. Under the microscope, alternating bands of
574 chlorite and quartz-sericite form the cleavage, which surrounds deformed
575 porphyroclasts of plagioclase, alkali-feldspar and minor quartz, and volcanic rock
576 fragments with devitrified groundmass. Plagioclase crystals are deformed, stretched,
577 and in general altered to sericite and epidote. Quartz porphyroclasts reveal
578 embayments. The chloritic bands are probably derived from altered pumiceous
579 horizons and are associated with abundant euhedral epidote in aggregated prismatic
580 crystals, mostly pistacite. These aggregates have variable sizes but reach up to 200
581 μm, and in general replace plagioclase. The quartz-sericite bands are formed by a
582 very fine mass of quartz, feldspars and abundant sericite, with minor chlorite. The
583 quartzo-feldspathic material has grain-shape preferred orientation parallel to the

foliation dipping moderately SW, revealing incipient bulging in quartz. Metamorphic minerals comprise chlorite, epidote, sericite, quartz, and calcite.

The breccias (Fig. 3D) consist of angular clasts of acidic volcanic rock (dominantly), with sizes from a few millimetres to more than 6 cm, in a very fine or sandy matrix that bears a finely spaced foliation. These rocks crop out at several places (e.g., CD12), and conspicuously in the area of Paso de las Lagunas and Paso Baqueano Catalán, where they are intercalated with metapsammites, slates and micaceous-chloritic phyllites. The breccias have abundant matrix and variable amounts of clasts of quartz and feldspars, and rock fragments (volcanic rock, slate, granite), mostly angular and with poor sorting. The clasts are usually highly flattened and stretched; at some outcrops (e.g., CD28), cigar-shaped clasts form part of a fabric that resembles L- or SL-tectonites.

Microscopic examination of the finer breccias reveals large clasts of very coarse sand or gravel immersed in an abundant (>30%) matrix. The matrix is formed by coarse sandstone and abundant very fine sand and silt, overprinted by very fine metamorphic sericite. Orientated sericite and flattened and stretched clasts, surrounded by anastomosed pressure-solution seams, define the tectonic foliation, which is closely spaced (micro-disjunctive) in the finer matrix. The microlithons in this fine matrix are weakly to completely orientated (Fig. 3E, F). A younger superposed foliation, formed by a zonal crenulation, is developed in the finer grained or micaceous parts of the sample (e.g. within metapelitic clasts), especially near thrust zones (see below).

Clasts are angular or subangular-to-subrounded, formed dominantly by quartz, feldspars, and fragments of volcanic or sedimentary rock. The volcanic rock fragments are either felsitic or mafic groundmass, the latter with very fine chlorite,

609 epidote and plagioclase. The sedimentary rock fragments are pelitic, with very fine
610 metamorphic sericite orientated parallel to the tectonic foliation. Less abundant
611 components include metamorphic rock fragments. We highlight the occurrence of
612 clasts of metamorphic rocks with an inherited foliation, in some cases oblique to the
613 foliation in the breccia. Some of these are fine-grained metasedimentary rock formed
614 by aligned sericite and muscovite, and others fine schists of granoblastic quartz and
615 micas (Fig. 3E, F). Additional clasts with phaneritic granoblastic texture containing
616 perthitic feldspar and quartz, and euhedral muscovite, may be acid igneous intrusive
617 rock fragments such as granite. Frequent flattened and stretched fragments of
618 crystalline chlorite and anhedral quartz are probably altered pumice. Detrital
619 muscovite is also present. Minor components include titanite, zircon, and detrital
620 biotite with pseudomorphic replacement by chlorite.

621 The metapsammites and slates form extensive outcrops interfingered with the
622 other facies. In the slates and phyllites, the stratification is usually transposed by the
623 main cleavage, with development of a distinct stretching lineation (Fig. 4A, B). In the
624 northeastern portion of our map area the foliation dips consistently SW (Fig. 2), but
625 towards Paso de las Lagunas the foliation has a more northerly strike, with dominant
626 westward low-angle dips. The stretching lineation plunges SW. Metapsammites
627 have a well-developed spaced foliation, anastomosed in the coarser facies, and
628 axial-planar to tight folds (sample CD10; Fig. 3G). The slates characteristically reveal
629 stretched and flattened ellipsoidal pyroclastic fragments, resembling altered
630 accretionary pellets.

631 Under the microscope, the metapsammites reveal poorly sorted angular-
632 subangular clasts up to 0.4 mm. The matrix is coarse silt with abundant metamorphic
633 chlorite and sericite. The sand clasts have sutured or lobate boundaries, with no

visible pores between them. The main components are quartz, sericitized plagioclase, and alkali-feldspar with partial albitization. Subordinate components are metamorphic rock fragments with granoblastic texture (quartz with subgrain rotation recrystallization) and metasedimentary rock fragments that reveal a fine continuous foliation. Even though many of these clasts are flattened and orientated parallel to the cleavage in the metapsammites, some of them evidence a pre-existing tectonic foliation (sample CD06; Fig. 3H). There are minor amounts of detrital muscovite and altered biotite, usually flattened between more competent grains. Some muscovite grains have a magmatic or metamorphic origin, as revealed by their inclusion into granoblastic polycrystalline quartzo-feldspathic fragments. Titanite and zircon are present as accessory minerals. Modal determinations in two samples reveal 26% and 12% alkali-feldspar, 33% and 50% plagioclase, 41% and 36% quartz, and 2% metasedimentary rock.

The disjunctive foliation in the metapsammites is variably developed, formed by anastomosed pressure-solution seams and abundant orientated fine sericite and quartz, both replacing the sedimentary matrix and forming strain fringes and necks in microboudinaged clasts. Orientated, very fine biotite or stilpnomelane also form in the cleavage domains. Very fine disseminated epidote and less-frequent calcite complete the metamorphic paragenesis.

The dominant structural fabric in the footwall of the Glaciar Marinelli Thrust is a tectonic foliation defined by the grain-shape preferred orientation of porphyroclasts, orientated metamorphic minerals such as sericite and chlorite, and pressure-solution seams (Figs. 3 and 4). Macroscopically, this foliation is clearly distinguished as a schistosity in the less-competent rocks, but is not as well developed in competent rocks such as cemented sandstones and rhyolite. In the

659 less competent metasedimentary rocks, the foliation transposes the original
660 sedimentary layering (e.g., Fig. 4A). In intensely deformed horizons, stretched
661 porphyroclasts and metamorphic phyllosilicates are orientated such that they form a
662 stretching lineation (Fig. 4B). We label this foliation S1, and the stretching lineation
663 L1. We find both fabrics comparable to foliation S1 and lineation L1 of Klepeis (1994)
664 in the footwall domain, and with S1 and L1 mapped by Nelson *et al.* (1980) in
665 northern Cordillera Darwin (Table 2). Away from the Glaciar Marinelli Thrust, near
666 Cerro Skottsberg, S1 has a NW-SE strike and dips moderately SW, being subparallel
667 to the tectonic grain in the region. Towards the Glaciar Marinelli Thrust, S1 seems
668 to be tilted by major folding, with a near N-S strike and gentle dips either to the west
669 (mostly) or east. Folding of S1 is evident near or within shear zones, as described
670 below.

671 Brittle-ductile thrusts are frequent in the footwall domain, characterized by
672 fault zones several metres thick (Fig. 4C), orientated from ENE-WSW to ESE-WNW.
673 Shear sense indicators such as deflected sigmoidal S1 foliation along shear bands
674 reveal consistent top-to-north kinematics (Fig. 4D, E). These deflections, as well as
675 asymmetric folds of the S1 foliation (Fig. 4F, G), are conspicuous within and near
676 the brittle-ductile fault zones, and are dominantly orientated parallel to these zones,
677 with variable hinge attitudes. Towards the Glaciar Marinelli Thrust, this folding of S1
678 surfaces is more intense and manifests microscopically as a zonal crenulation
679 cleavage, which constitutes a macroscopic smooth to anastomosed spaced foliation
680 with crenulation folds visible in the microlithons (Fig. 4H). This foliation is labelled S2
681 in this work and is comparable to foliation S3 from Klepeis (1994; Table 2). The
682 associated F4 folds described by this author are the crenulation folds and sigmoidal
683 deflections formed near shear bands in brittle-ductile thrust zones, which we label

F2. The intersection of S2 with S1 surfaces forms a crenulation lineation (L2), which is subparallel to F2. We did not recognize the fine-spaced cleavage at low angle to S1 briefly mentioned by Klepeis (1994), which he labels S2. Accordingly, our S2 foliation corresponds to the S2 foliation of northern Cordillera Darwin (Nelson *et al.*, 1980; Table 2).

4.1.2. Hanging wall of the Glaciar Marinelli Thrust

The Glaciar Marinelli Thrust manifests as a brittle-ductile fault zone characterized by brecciated rock, with profuse quartz veins. The outcrop width is at least 10 to 20 m, partly covered by debris, and distinguished in the field as a prominent escarpment in the western flank of the Cañadón del Horno headwaters (Fig. 5A, B). The escarpment has a WNW-ESE trend (Fig. 2). The fault affects fine phyllites and breccias, the latter similar to those described in the footwall. Profuse shear bands with sigmoidal deflection in the dominant foliation (see below) indicate a top-to-north/northeast shear sense, as reported by Klepeis (1994; Fig. 5C, D). Discrete brittle faults cut the previous foliations within the brittle-ductile fault zone.

For at least one kilometre (between CD05 and CD25), the hanging wall of the fault is composed of the same metasedimentary phyllites and fine schists. These rocks reveal a finely spaced foliation, more or less micaceous, which clearly affected the original sedimentary layering (S0). The sedimentary layering is folded into isoclinal folds (F1) and is mostly transposed by the dominant foliation, which is the same S1 foliation that was described in the footwall (Fig. 5E-H). The microlithons of S1, therefore, comprise rootless F1 folds and discontinuous S0 bands (Fig. 5E). The S1 foliation is also affected by the S2 crenulation foliation and F2 folds, which are very well developed near brittle-ductile thrust faults (Fig. 5D), as observed at CD25

709 and CD05. In general, the studied transect in the hanging wall of the Glaciar Marinelli
710 Thrust reveals a more profuse development of S2 than the footwall. In some
711 exposures, the S2 foliation is variably developed at outcrop scale, showing horizons
712 where it completely transposes S1, and others of equivalent thickness where it
713 becomes more widely spaced (Fig. 6A-C).

714 The sedimentary layering in the phyllites is formed by alternating stripes of
715 lighter quartz-rich material and darker very fine material, which is recognized in the
716 microlithons of the S1 transposition foliation, especially in the hinges of rootless F1
717 folds (Fig. 5E, G). Under the microscope, the lighter bands are composed of fine
718 metapsammite horizons, with grains smaller than 200 μm and in general smaller
719 than 50 μm of quartz and feldspar (mostly plagioclase; Figs. 5F-H and 6D-H). Quartz
720 reveals grain size reduction due to dynamic recrystallization by subgrain rotation,
721 which results in new individuals of 20 to 30 μm, with polygonal grain boundaries.
722 Some of these polygonal boundaries appear affected by subsequent bulging
723 recrystallization that modifies them into lobulated boundaries.

724 These metasedimentary rocks are cut by coarse quartz veins, which show
725 both oblique and subparallel boundaries with the metapsammites, although the
726 original contacts are highly deformed and partially recrystallized (Figs. 5G-H and 6G-
727 H). The quartz in the veins has sizes up to 0.5–0.6 mm, with polygonal or rectilinear
728 grain boundaries affected by later bulging (as mentioned for the metapsammites),
729 and reveals undulose extinction and subgrain formation. Acicular muscovite within
730 the quartz crystals produces pinning structures in some grain boundaries.
731 Occasional chlorite fibres are included in these quartz veins.

732 Both the metapsammite and the quartz veins are intercalated with bands of
733 metapelite, in which the fine protolith is replaced by metamorphic euhedral

muscovite with preferred orientation, less dominant chlorite (also euhedral in fibres or aggregates), and euhedral biotite porphyroblasts (Figs. 5F-H and 6F-H). Alteration in the biotite produces a faint coloration and, in some cases, it is replaced by pseudomorphic chlorite. Accessory minerals include many detrital zircon grains.

In agreement with the macroscopic observations, the microstructure reveals rootless isoclinal F1 folds in the banded metapsammite-metapelite horizons denoting the original stratification (S0), as well as in the quartz veins (Fig. 5F-H). The S1 transposition foliation is well developed, parallel to F1 axial traces, and defined by the orientated metamorphic muscovite, chlorite, and biotite, and pressure-solution seams. These metamorphic minerals thus formed coevally with development of S1 and F1, together with the granoblastic texture of the veins and the polygonal grains of the metapsammite bands. The latter are clearly affected by subsequent lower grade deformation and dynamic recrystallization, reflected by the deformed quartz with lobulated boundaries that obliterate the prior rectilinear boundaries.

A zoned S2 crenulation foliation deforms both the F1 folds and S1 foliation, forming F2 folds (Fig. 6D-H). A sample from CD23 clearly illustrates the relationship between F2/S2 and the prior fabrics. We cut two thin sections from this sample, one from the hinge zone of an F2 fold (Fig. 6D), and the second from the “long” back-limb of the same fold (Fig. 6E). In Fig. 6E a clear subparallel relationship between S0 and S1 is observed, as well as the metasedimentary texture of the protolith. The S1 foliation has smooth cleavage domains 0.1–0.2 mm thick, preferentially formed in the transposed metapelitic protolith, that separate 1.4–0.4 mm thick microlithons. The latter are formed by bands of metapsammite, with fine sand-silt grains of quartz and feldspar, large detrital muscovite grains, and a completely orientated fabric. The microlithons have less abundant fine muscovite-sericite, chlorite and biotite.

759 Discontinuous pressure-solution seams in the microlithons are parallel to the S1
760 foliation. In this long limb of F2, S2 develops as a zonal crenulation, spaced 0.08–
761 0.3 mm at a low angle with respect to S1 (~25°). It has minor, new orientated sericite
762 and occasional biotite, both very fine, in the cleavage domains.

763 Metapsammitic layers within microlithons of S1 form the thin section cut from
764 the hinge zone of the F2 fold (Fig. 6D). They have variable thicknesses between 40
765 and 240 μm, being thicker in the hinges of F2 microfolds, and with the same
766 mineralogical characteristics described for figure 6E, including oversized detrital
767 muscovite obliquely orientated compared to metamorphic muscovite-sericite. In this
768 sample, S2 is a well-developed discrete foliation, crosscutting S1 in the limbs of the
769 F2 microfolds (Fig. 6E). The S2 cleavage domains have a variable spacing
770 depending on the size of the clasts, which can be as small as 10–30 μm. They reveal
771 new sericite in a smooth to anastomosed foliation, abundant pressure-solution
772 seams, and some grain-shape preferred orientation of quartz in the hinges of the F2
773 microfolds. In the microlithons, there is a strong to moderate orientation of the
774 components.

775 It is necessary to compare these structures with those described by Klepeis
776 (1994) in the hanging wall of the Glaciar Marinelli Thrust (see Table 2 and section
777 2.3). The “early” S1 foliation described by this author is a combination of the original
778 metapelitic-metapsammitic layering and quartz veins that we describe above (S0),
779 and the subparallel or transposition foliation (S1). Accordingly, the isoclinal folds
780 called F2 by Klepeis (1994) are the F1 folds that we recognized in the S0 and the
781 quartz veins (Fig. 5E-H). The “dominant” S2 foliation described by Klepeis (1994) as
782 a crenulation cleavage overprinting his S1 and axial-planar to his F2, is coplanar with
783 the S1 foliation recognized in the footwall of the Glaciar Marinelli Thrust. This

784 “dominant” foliation is thus parallel to our isoclinal F1 folds, and is therefore the S1
785 transposition foliation that we observe in the field and describe in our thin sections
786 (Fig. 5E-H): it is the same S1 foliation present in the footwall of the thrust.
787 Accordingly, the S3 crenulation of Klepeis (1994) corresponds to our S2, which is
788 associated with folding (his F3, equal to our F2; Fig. 6). According to Klepeis (1994),
789 shear bands with top-to-northeast shear sense (F4 in his work) bend these folds and
790 crenulation. These are the same shear bands described here, associated with the
791 F2 folds and deflected S1 in the brittle-ductile shear zones (Fig. 5C, D).

792 In summary, the same structural generations recognized in the footwall are
793 present in the hanging wall. The key to defining this structural sequence is the
794 recognition of the transposed metasedimentary bands as the primary S0 of the
795 protolith.

796

797 **4.2. Geochronological results**

798 ***4.2.1. Sample CD05, metasedimentary phyllite from the hanging wall***

799 Unfortunately, very few zircon grains could be retrieved from sample CD05:
800 45 were analysed (Supplementary File 2). They were imaged by
801 cathodoluminescence images (Supplementary File 5) and show different sizes and
802 shapes, from sub-euhedral to sub-rounded. The grains yield variable U and Pb
803 contents (81–3155 ppm and 58–4711 ppm, respectively), Th/U ratios (0.03 to 0.6),
804 as well as apparent ages (447 to 1886 Ma). In a KDE diagram (Fig. 7A), the ages
805 define three main peaks: around 1000, 770, and 530 Ma. These zircon grains are
806 detrital in origin, with a few (n=5) yielding metamorphic Th/U ratios below 0.1
807 (apparent ages of 1886±12, 1202±24, 973±42, 625±23, and 447±20 Ma), while most

808 have Th/U ratios compatible with a magmatic origin (Th/U>0.1). For this sample the
809 YSG and Y3Go ages are Ordovician, 447±20 Ma and 471±12 Ma, respectively (Fig.
810 7A; Supplementary File 2), while the MLA is less precise and within error of these
811 calculations at 454±28 Ma.
812
813 ***4.2.2. Sample CD06, metapsammite from the footwall***
814
815 Sample CD06 provided numerous zircon grains, from which we analysed 111
816 (Supplementary File 2). As for sample CD05, the cathodoluminescence images
817 (Supplementary File 6) display various shapes and sizes for the zircon grains, from
818 euhedral to rounded. They have variable U and Pb contents (21 to 2589 ppm and
819 20 to 4187 ppm, respectively), as well as Th/U ratios (0.01 to 1.12), suggesting that
820 nine grains have a metamorphic origin with ages of ca. 1270, 800–770, 640–600,
821 and 580–520 Ma. The remaining grains yield magmatic signatures. These
822 observations indicate that the zircon grains were derived from different rock types,
823 underscoring their detrital origin. They yielded apparent ages from 309 Ma to 3535
824 Ma. The KDE diagram shows several age peaks, the three main ones at 610, 520,
825 and 400 Ma (Fig. 7B). For this sample, the YSG age is 309±9 Ma (late
826 Carboniferous) while the Y3Go age is 336±5 Ma (early Carboniferous) (Fig. 7B;
827 Supplementary File 2). The MLA is intermediate at 314±11 Ma.

828 **5. Discussion**

829 **5.1. Structural generations and deformation sequence in the study area**

830 Table 2 shows the correlation between the structures previously described in
831 our study area, and those recognized in our work. As can be noticed, we identified

832 the same generations of structures as Klepeis (1994; S1 and S2-F2) in the footwall
833 of the Glaciar Marinelli Thrust, except for a "*fine spaced cleavage at low angle to*
834 *S1*". We do not know the meaning of this later fabric, which is not clearly described
835 by the mentioned author and we did not recognize it in the field or in thin section. In
836 the hanging wall of the thrust, we noticed the same generations as in the footwall.
837 However, according to Klepeis (1994) there is an additional and older tectonic fabric
838 (S1 in his work), which he considered part of the pre-Andean Db deformation of
839 Nelson *et al.* (1980; Table 2). As established in section 4.1, this early fabric has been
840 confused with the transposed S0, which is dismembered and isoclinally folded,
841 forming discontinuous bands subparallel to the main transposition S1 (Fig. 5E-H).
842 This confusion could have influenced the assignment of the hanging wall rocks to
843 the basement units in previous work. Therefore, it is critical to determine the precise
844 generation of structures in that area.

845 Our work shows that the same structural events affected the hanging wall and
846 footwall of the Glaciar Marinelli Thrust. The sequence of deformation comprises a
847 first ductile deformation producing the main cleavage (S1), which varies from a
848 spaced cleavage in more competent rocks (rhyolites, metapsammites) and a
849 transposition cleavage in phyllites and slates (Fig. 8A, B). The transposition cleavage
850 is clearly manifested in the more deformed rocks of the hanging wall, where the
851 original sedimentary lamination (S0) remains as rootless isoclinal folds between
852 cleavage domains (Fig. 5E-H). This deformation was coeval with, or slightly
853 preceded, the higher metamorphic grade revealed by euhedral biotite
854 porphyroblasts (Figs. 5F-H and 6F-H). The subsequent deformation resulted in
855 brittle-ductile thrusts such as the Glaciar Marinelli Thrust (Fig. 8C). These shear
856 zones were accompanied by folding and crenulation of the prior S1 fabrics forming

857 the S2 crenulation foliation, F2 folds, and related structures (Figs. 4D-H, 5C-D, and
858 6). This deformation occurred without significant metamorphism.

859 These two structural generations reflect the known history of deformation
860 elsewhere in the Fuegian Andes: a ductile contractional deformation, associated with
861 the closure of the Rocas Verdes Basin ($D1_{CB}$), and the subsequent development of
862 the Fuegian thrust-fold belt ($D2_{CB}$), as mentioned in section 2.1 (Fig. 8). The rocks
863 studied in this work show no deformation prior to $D1_{CB}$ structures, suggesting either
864 that 1) these rocks are Paleozoic basement without pre-Jurassic deformation, or that
865 2) they comprise part of the sedimentary and volcanic deposits of the Rocas Verdes
866 Basin. We consider that the first possibility is highly improbable, since it would imply
867 that these rocks covering the Upper Devonian Svea granite remained without any
868 trace of penetrative deformation until the Late Cretaceous closure of the Rocas
869 Verdes Basin. In other words, they would have persisted ca. 260 Myr in the SW
870 margin of Gondwana unaffected by the proposed late Paleozoic-early Mesozoic
871 episodes of regional deformation in that margin (e.g. Ramos, 2008; Castillo *et al.*,
872 2017; Riley *et al.*, 2023). This is very unlikely, and local basement rocks are indeed
873 deformed by pre-Jurassic penetrative structures (Nelson *et al.*, 1980; Klepeis *et al.*,
874 2010; Hervé *et al.*, 2010a). We conclude that the studied rocks form part of the Rocas
875 Verdes Basin cover.

876

877 **5.2. Stratigraphy of the footwall and hanging wall rocks of the Glaciar Marinelli**
878 **Thrust**

879 The problem of distinguishing between cover rocks and basement in
880 Cordillera Darwin is an issue documented since early geological work in the area

(Kranck, 1932; Fester, 1938). This is especially so for fine-grained metasedimentary rocks, since coarser rocks in the cover may bear foliated clasts interpreted as eroded basement. For example, despite Kranck (1932) repeatedly describing “old basement schists” or “high metamorphic schists” as dominantly quartz-micaceous fine schists, he also recorded these facies intermingled with the Tobífera Formation in the fjords of northern Cordillera Darwin and with coarser facies in the Lapataia Formation (see section 2.2.1). Subsequent work included some of these fine schists either within the basement or within the cover rocks, as we can observe comparing maps and sample descriptions from Nelson *et al.* (1980), Johnson (1990), and Ortiz (2007).

The usage of geochronological dating, especially U-Pb dating in zircons, has provided valuable information on the nature and origin of the rocks in this region. However, sediments deposited above the basement without particularly profuse synchronous volcanism (e.g., in a synrift environment), are likely to reflect zircon ages of the eroded basement instead of syndepositional ages (Cawood *et al.*, 2012; Copeland, 2020; Castillo *et al.*, 2022). This has been reported for the Mesozoic cover rocks of the Fuegian Andes (Hervé *et al.*, 2010a; Cao *et al.*, 2022, 2025), and in similar back-arc or rift settings (Rossignol *et al.*, 2019). In this context, detailed petrographic studies are crucial to complement the geological significance of geochronological determinations.

Hervé *et al.* (2010a) proposed a working hypothesis for distinction between cover and basement within the northern Cordillera Darwin Metamorphic Complex, arguing that samples with Permian or Triassic zircons and without Jurassic zircons can be considered part of the Rocas Verdes Basin, whilst samples with Carboniferous or older ages may be part of the basement. They advised caution regarding this presumption, however, and we indeed consider that it is challenged

by the evidence from the Lapataia Formation (see below), but also from rocks within the Cordillera Darwin Metamorphic Complex that bear sparse Jurassic grains, and abundant zircons with ages older than the Permian (Hervé *et al.*, 2010a; see Table 3). All these samples have scarce but sufficient petrographic or geochronological evidence that proves they belong to the Mesozoic cover, having sparse or no late Paleozoic or Triassic zircon grains. Thus, lower Paleozoic rocks have to be considered as important sources for detrital zircons in the Rocas Verdes Basin fill, as can be inferred from the ages of the metamorphic zircons in our dataset. Conversely, to use the lack of Permo-Triassic age signatures in a rock as evidence that this rock belongs to the basement, is disputable.

Petrographic analysis of the rocks studied in this work reveals facies comparable to the Tobífera Formation and Lemaire Complex (i.e. volcanic, volcaniclastic, and sedimentary rocks), and with the Lapataia Formation (metasedimentary and metabasic rocks). The former are distributed in the footwall of the Glaciar Marinelli Thrust, including the Estratos Paso de las Lagunas of Mella and Quiroz (2023), previously mapped as the La Paciencia Formation by Klepeis (1994; Table 1; Supplementary File 1). We consider that the facies shown in figure 4 are significant enough to discard the latter argument, since the La Paciencia Formation is mostly metapelitic according to Cortés and Valenzuela (1960) and later work (see Cañón, 2000).

As defined by Mella and Quiroz (2023), the Estratos Paso de las Lagunas are composed of metasedimentary rocks, including quartzites and metaconglomerates, unconformably covering the Upper Devonian Svea granite and an associated early Carboniferous orthogneiss. Sample CD06 from Paso de las Lagunas is a metapsammite intercalated with breccias that yields a Carboniferous MDA (between

ca. 339 and 310 Ma, depending on the MDA calculation method used), and a rather continuous record of detrital Paleozoic ages with a marked late Neoproterozoic-Cambrian peak. An older peak contains late Grenvillian Neoproterozoic ages (~0.8–1.0 Ga; Fig. 7B). We consider the facies of sample CD06 to be very closely similar to that of the Lemaire Complex and Tobífera Formation along the northern flank of Cordillera Darwin and in Argentina (Johnson, 1990; Olivero and Martinioni, 1996; Ortiz, 2007; Hervé *et al.*, 2010a). This interpretation is made notwithstanding the Paleozoic detrital zircon ages and is consistent with similar interpretations elsewhere in the region. Notice for example the metasandstone of sample FO0524 described by Ortiz (2007), with foliated metamorphic rock fragments comprising 25% of the sample, and dated by Hervé *et al.* (2010a; see Table 3). Despite its Triassic MDA and prominent Cambrian age peak, and the lack of Jurassic ages, this rock is very likely part of the sedimentary fill of the Rocas Verdes Basin.

Sample CD06 also reveals clasts of metamorphic rocks, alike other sandstones and breccias cropping out in the footwall of the Glaciar Marinelli Thrust (Fig. 3E, F, H), a feature that has been also recognized in the Lapataia Formation and in the Lemaire Complex (Cao *et al.*, 2022, 2025). The Lemaire Complex sandstones exposed in the footwall of the Mina Beatriz thrust (Fig. 1), for example, described by Olivero and Martinioni (1996), reveal clasts of foliated rocks and are interlayered with tuffs and rhyolites. In a similar way, the interlayered metatuffs and rhyolite in the metasedimentary succession of Paso de las Lagunas suggests the assignment of these rock exposures to the Tobífera Formation (Fig. 2). This leaves the explanation of the Paleozoic U-Pb detrital zircon ages of sample CD06 as a signature derived from the prominent supply of detritus from eroded basement rocks,

955 probably influenced by the nearby Svea granite, as shown schematically in figure
956 8A.

957 Likewise, the phyllites of the hanging wall of the Glaciar Marinelli Thrust are
958 composed of facies that resemble the phyllites and schists of the Lapataia Formation
959 in Argentina. The latter is well known in the hanging wall of the Mina Beatriz thrust,
960 which has been traced regionally and correlated with the Glaciar Marinelli Thrust
961 (Cao *et al.*, 2022, 2023; Fig. 1). Previous work in our study area assigned the rocks
962 in the hanging wall of the Glaciar Marinelli Thrust to the basement (Klepeis, 1994;
963 Supplementary File 1) or to the Cordillera Darwin Metamorphic Complex (Rojas and
964 Mpodozis, 2006; Hervé *et al.*, 2010a). Similarly, the Lapataia Formation has been
965 considered part of the Paleozoic basement of the Fuegian Andes for many years
966 (Kranck, 1932; Borrello, 1972; Bruhn, 1979). However, recent work established its
967 inclusion in the Mesozoic cover based on the absence of a pre-Andean foliation and
968 the occurrence of deformed, foliated, inherited rock fragments within the Formation
969 (Cao *et al.*, 2018, 2022). The strata cropping out in the hanging wall of the Glaciar
970 Marinelli Thrust show the same petrographic and microstructural characteristics, as
971 mentioned in previous sections. Regardless of the calculation method used for the
972 MDA, sample CD05 from the hanging wall rocks yields an Ordovician MDA, and
973 older clusters of latest Neoproterozoic-early Cambrian and ~1.1–0.8 Ga age groups
974 that are comparable to those observed in sample CD06 (Fig. 7). These age clusters
975 are also comparable to the ages found in the Lapataia Formation (Cao *et al.*, 2022),
976 consistent with the provenance from an eroded Paleozoic basement during the early
977 development of the Mesozoic syn-rift deposits in the absence of coeval volcanism
978 (Fig. 8A). The lack of younger Paleozoic zircons, compared with sample CD06,

reveals different source areas within the Jurassic basin and probably different structural levels, prior to reverse faulting along the Glaciar Marinelli Thrust.

Neoproterozoic-Cambrian and Grenvillian zircons are largely documented in basement rocks and in the detrital record of the Mesozoic cover of the Fuegian Andes (e.g., Hervé *et al.*, 2010a). Recent paleogeographic reconstructions of Gondwana assembly propose a Neoproterozoic-Cambrian arc on the paleo-Pacific margin of the East Antarctica craton, which was located adjacent to the north Patagonian and south Patagonian (Magallanes Basin basement) blocks (González *et al.*, 2018). Older zircons, derived from eroded Grenvillian mobile belts, are expectedly abundant in the basement of these blocks.

6. Conclusions

Detailed petrographic and structural observations in the hanging wall of the Glaciar Marinelli Thrust reveal Late Cretaceous-Cenozoic ductile ($D1_{CB}$) and brittle-ductile ($D2_{CB}$) structures, associated with the closure of the Rocas Verdes Basin and later development of the Fuegian thrust-fold belt. No older structures were recognized, and previous interpretations of a “pre-Jurassic” deformation in these rocks were probably influenced by the difficult recognition of the transposition of the original sedimentary layering by the Late Cretaceous $D1_{CB}$ (S1) main foliation. We identify the same structure generations in the metasedimentary-metavolcanic sequence exposed in the footwall of the Glaciar Marinelli Thrust.

These structural relationships, as well as the facies of the rocks in our study area, indicate that these are metasedimentary rocks of the Rocas Verdes Basin cover. Accordingly, the footwall rocks reveal protolith facies identical to those

recognized in the Tobífera Formation-Lemaire Complex (Middle Jurassic-Berriasian), which include rhyolite, breccias, sandstones and finer facies (tuffs and pelite). In the hanging wall, breccias and fine metasedimentary rocks with a higher degree of deformation resemble the facies recognized in the Jurassic Lapataia Formation. The detrital zircons obtained from two samples in these units have Ordovician and Carboniferous youngest U-Pb ages, and several older age peaks, indicative of a sediment source in basement highs exposed during syn-rift deposition. The Upper Devonian Svea Granite is an excellent example of such basement exposures in our study area. This work emphasizes the need for detailed petrographic and structural analyses to complement geochronological studies, when aiming to make stratigraphic determinations in rocks with relatively scarce synsedimentary volcanism.

Acknowledgements

This research was funded by ANID through Project Fondecyt 1231211 to FP. We thank CONAF and Cuerpo Militar del Trabajo (CMT) for sampling permission at Yendegaia National Park, Sra. Ivette from Caleta María for logistic support and Sr. César for his hospitality. We also want to thank V. Mosqueira González for help during fieldwork and for granting usage of some of the photographs. Thin sections were prepared by L. Remón (CADIC-CONICET). We thank D. Barbeau, V. Muller, guest editor R. Pankhurst, and editor D. Bertin for their constructive reviews.

References

Álvarez-Marrón, J.; McClay, K.; Harambour, S.; Rojas, L.; Skarmeta, J. 1993. Geometry and evolution of the frontal part of the Magallanes foreland thrust and fold belt (Vicuña Area), Tierra del Fuego, Southern Chile. AAPG Bulletin 77: 1904-1921.

Betka, P.; Klepeis, K.; Mosher, S. 2015. Along-strike variation in crustal shortening and kinematic evolution of the base of a retroarc fold-and-thrust belt: Magallanes, Chile 53°S-54°S. Geological Society of America Bulletin 127(7-8): 1108-1134.

Betka, P.; Mosher, S.; Klepeis, K. 2022. Progressive Development of a Distributed Ductile Shear Zone beneath the Patagonian Retroarc Fold-Thrust Belt, Chile. Lithosphere 2022(1): 3820115.

Borrello, A. 1972. Cordillera Fueguina. *In* Geología Regional Argentina. Academia Nacional de Ciencias: 741-754. Córdoba.

Bruhn, R.L.; Stern, C.R.; de Wit, M.J. 1978. Field and geochemical data bearing on the development of a Mesozoic volcano-tectonic rift zone and back-arc basin in southernmost South America. Earth and Planetary Science Letters 41(1): 32-46.

Bruhn, R.L. 1979. Rock structures formed during back-arc basin deformation in the Andes of Tierra del Fuego. Geological Society of America Bulletin 90(11): 998-1012.

Calderón, M.; Fildani, A.; Hervé, F.; Fanning, C.M.; Weislogel, A.; Cordani, U. 2007. Late Jurassic bimodal magmatism in the northern sea-floor remnant of the

Rocas Verdes basin, southern Patagonian Andes. Journal of the Geological Society, London 164: 1011-1022.

Cañón, A. 2000. Nuevos antecedentes en la estratigrafía de la Cuenca de Magallanes. Anales Instituto de la Patagonia 28: 41-50.

Cao, S.J.; Torres Carbonell, P.J.; Dimieri, L.V. 2018. Structural and petrographic constraints on the stratigraphy of the Lapataia Formation, with implications for the tectonic evolution of the Fuegian Andes. Journal of South American Earth Sciences 84: 223-241.

Cao, S.J.; Torres Carbonell, P.J.; Bordese, S.; Lovecchio, J.P. 2022. Early rifting during marginal basin development: Petrography, microstructure, and detrital zircon U-Pb geochronology of the Lapataia Formation, Argentine Fuegian Andes. Basin Research 34(4): 1400-1420.

Cao, S.J.; Torres Carbonell, P.J.; Sánchez, N.P.; Bordese, S.; Dimieri, L.V. 2023. Thrust tectonics in the Fuegian Andes central belt: A detailed geometric-kinematic analysis and new thermochronological constraints. Tectonophysics 862: 229966.

Cao, S.J.; González Guillot, M.; Torres Carbonell, P.J.; Bordese, S.; Lovecchio, J.P.; Dimieri, L.V. 2025. Stratigraphy of the Rocas Verdes basin: Petrography and new U-Pb ages from the Argentine Fuegian Andes. Journal of South American Earth Sciences 152: 105315.

Castillo, P.; Fanning, C.M.; Pankhurst, R.J.; Hervé, F.; Rapela, C. 2017. Zircon O- and Hf-isotope constraints on the genesis and tectonic significance of Permian magmatism in Patagonia. Journal of the Geological Society 174(5): 803-816.

1072 Castillo, P.; Bahlburg, H.; Fernandez, R.; Fanning, C.M.; Berndt, J. 2022. The
1073 European continental crust through detrital zircons from modern rivers:
1074 Testing representativity of detrital zircon U-Pb geochronology. Earth-Science
1075 Reviews 232: 104145.
1076 Cawood, P.A.; Hawkesworth, C.J.; Dhuime, B. 2012. Detrital zircon record and
1077 tectonic setting. Geology 40(10): 875-878.
1078 Copeland, P. 2020. On the use of geochronology of detrital grains in determining the
1079 time of deposition of clastic sedimentary strata. Basin Research 32(6): 1532-
1080 1546.
1081 Cortés, R.; Valenzuela, H. 1960. Estudio geológico del área Lago Blanco - Hito XIX
1082 - Monte Hope (porción sur-central de Tierra del Fuego). Empresa Nacional
1083 del Petróleo. Punta Arenas. 22 pp.
1084 Coutts, D.S.; Matthews, W.A.; Hubbard, S.M. 2019. Assessment of widely used
1085 methods to derive depositional ages from detrital zircon populations.
1086 Geoscience Frontiers 10(4): 1421-1435.
1087 Cunningham, W.D. 1994. Uplifted ophiolitic rocks on Isla Gordon, southernmost
1088 Chile: implications for the closure history of the Rocas Verdes marginal basin
1089 and the tectonic evolution of the Beagle Channel region. Journal of South
1090 American Earth Sciences 7(2): 135-147.
1091 Cunningham, W.D. 1995. Orogenesis at the southern tip of the Americas: the
1092 structural evolution of the Cordillera Darwin metamorphic complex,
1093 southernmost Chile. Tectonophysics 244(4): 197-229.
1094 Dalziel, I.W.D.; Elliot, D.H. 1971. Evolution of the Scotia Arc. Nature 233: 246-252.
1095 Dalziel, I.W.D.; de Wit, M.J.; Palmer, K.F. 1974. Fossil marginal basin in the southern
1096 Andes. Nature 250: 291-294.

Dalziel, I.W.D. 1986. Collision and Cordilleran orogenesis: an Andean perspective. Geological Society, London, Special Publications 19(1): 389-404.

Dalziel, I.W.D.; Brown, R.L. 1989. Tectonic denudation of the Darwin metamorphic core complex in the Andes of Tierra del Fuego, southernmost Chile: implications for Cordilleran orogenesis. Geology 17(8): 699-703.

de la Cal, H.G.; Lajoinie, M.F. 2023. Petrografía del Complejo Ígneo y Metamórfico de Tierra del Fuego en el subsuelo de la Cuenca Austral, Argentina. *In* 14° Congreso de Mineralogía, Petrología Ígnea y Metamórfica, y Metalogénesis, Actas: 302-305, Bahía Blanca.

Dickinson, W.R.; Gehrels, G.E. 2009. Use of U-Pb ages of detrital zircons to infer maximum depositional ages of strata: A test against a Colorado Plateau Mesozoic database. Earth and Planetary Science Letters 288(1): 115-125.

Fester, G. 1938. La Cordillera Darwin. Anales de la Sociedad Científica Argentina 126(2): 87-88.

González Guillot, M.; Urraza, I.; Acevedo, R.D.; Escayola, M. 2016. Magmatismo básico jurásico-cretácico en los Andes Fueguinos y su relación con la Cuenca Marginal Rocas Verdes. Revista de la Asociacion Geológica Argentina 73(1): 1-22.

González, P.D.; Sato, A.M.; Naipauer, M.; Varela, R.; Basei, M.; Sato, K.; Llambías, E.J.; Chemale, F.; Dorado, A.C. 2018. Patagonia-Antarctica Early Paleozoic conjugate margins: Cambrian synsedimentary silicic magmatism, U-Pb dating of K-bentonites, and related volcanogenic rocks. Gondwana Research 63: 186-225.

Hanson, B.; Wilson, T. 1991. Submarine rhyolitic volcanism in a Jurassic proto-marginal basin, southern Andes, Chile and Argentina. *In* Andean magmatism

and its tectonic setting, Geological Society of America Special Paper (Harmon, R.; Rapela, C.; editors). Geological Society of America: 13-27. Boulder.

Hervé, F.; Nelson, E.; Kawashita, K.; Suárez, M. 1981. New isotopic ages and the timing of orogenic events in the Cordillera Darwin, southernmost Chilean Andes. Earth and Planetary Science Letters 55(2): 257-265.

Hervé, F.; Fanning, C.M.; Pankhurst, R.J.; Mpodozis, C.; Klepeis, K.; Calderón, M.; Thomson, S.N. 2010a. Detrital zircon SHRIMP U-Pb age study of the Cordillera Darwin Metamorphic Complex of Tierra del Fuego: sedimentary sources and implications for the evolution of the Pacific margin of Gondwana. Journal of the Geological Society 167(3): 555-568.

Hervé, F.; Calderón, M.; Fanning, C.M.; Kraus, S.; Pankhurst, R.J. 2010b. SHRIMP chronology of the Magallanes Basin basement, Tierra del Fuego: Cambrian plutonism and Permian high-grade metamorphism. Andean Geology 37: 253-275.

Johnson, C. 1990. Antecedentes estratigráficos de la ribera Sur del Seno Almirantazgo. Tesis Memoria de Título (Unpublished), Universidad de Chile, Departamento de Geología y Geofísica: 122 p.

Katz, H.R. 1963. Revision of Cretaceous stratigraphy in Patagonian cordillera of Ultima Esperanza, Magallanes Province, Chile. AAPG Bulletin 47(3): 506-524.

Klepeis, K.A. 1994. Relationship between uplift of the metamorphic core of the southernmost Andes and shortening in the Magallanes foreland fold and thrust belt, Tierra del Fuego, Chile. Tectonics 13(4): 882-904.

1146 Klepeis, K.A.; Austin Jr., J.A. 1997. Contrasting styles of superposed deformation in
1147 the southernmost Andes. Tectonics 16(5): 755-776.
1148 Klepeis, K.A.; Betka, P.; Clarke, G.; Fanning, M.; Hervé, F.; Rojas, L.; Mpodozis, C.;
1149 Thomson, S. 2010. Continental underthrusting and obduction during the
1150 Cretaceous closure of the Rocas Verdes rift basin, Cordillera Darwin,
1151 Patagonian Andes. Tectonics 29(3): TC3014.
1152 Kohn, M.J.; Spear, F.S.; Dalziel, I.W.D. 1993. Metamorphic P-T Paths from
1153 Cordillera Darwin, a Core Complex in Tierra del Fuego, Chile. Journal of
1154 Petrology 34(3): 519-542.
1155 Kohn, M.J.; Spear, F.S.; Harrison, T.M.; Dalziel, I.W.D. 1995. 40Ar/39Ar
1156 geochronology and P-T-t paths from the Cordillera Darwin metamorphic
1157 complex, Tierra del Fuego, Chile. Journal of Metamorphic Geology 13(2):
1158 251-270.
1159 Kranck, E.H. 1932. Geological investigations in the Cordillera of Tierra del Fuego.
1160 Acta Geographica Societas Geographica Fenniae 4: 1-231.
1161 Lobo, C.; González Guillot, M.; Torres Carbonell, P.J.; Rodríguez, C.; Escayola, M.;
1162 Aragón, E.; Martín, G.; Garrido, C.J. 2024. Hallazgo de posible basamento de
1163 la cuenca Rocas Verdes en el sector Argentino de la Cordillera Fueguina. *In*
1164 XXII Congreso Geológico Argentino Actas: 365-366. San Luis.
1165 Maloney, K.T.; Clarke, G.L.; Klepeis, K.A.; Fanning, C.M.; Wang, W. 2011. Crustal
1166 growth during back-arc closure: Cretaceous exhumation history of Cordillera
1167 Darwin, southern Patagonia. Journal of Metamorphic Geology 29(6): 649-
1168 672.

1169 Martinioni, D.R.; Olivero, E.B.; Medina, F.A.; Palamarczuk, S.C. 2013. Cretaceous
1170 stratigraphy of Sierra de Beauvoir, Fuegian Andes (Argentina). Revista de la
1171 Asociación Geológica Argentina 70(1): 70-95.
1172 Mella, M.; Quiroz, D. 2023. Granito Svea: magmatismo Devónico-Carbonífero en
1173 Cordillera de Darwin, Tierra del Fuego, Chile. *In* XVI Congreso Geológico
1174 Chileno: 206. Santiago.
1175 Mukasa, S.B.; Dalziel, I.W.D. 1996. Southernmost Andes and South Georgia Island,
1176 North Scotia Ridge: Zircon U-Pb and muscovite 40Ar39Ar age constraints on
1177 tectonic evolution of Southwestern Gondwanaland. Journal of South
1178 American Earth Sciences 9(5–6): 349-365.
1179 Nelson, E.P.; Dalziel, I.W.D.; Milnes, A.G. 1980. Structural geology of the Cordillera
1180 Darwin - Collisional-style orogenesis in the southernmost Chilean Andes.
1181 Eclogae Geologicae Helvetiae 73: 727-751.
1182 Olivero, E.B.; Martinioni, D.R. 1996. Sedimentología de las Formaciones Lemaire y
1183 Yahgan (Jurásico-Cretácico) en Tierra del Fuego. *In* XIII Congreso Geológico
1184 Argentino y III Congreso de Exploración de Hidrocarburos, Actas 2: 45-59.
1185 Olivero, E.B.; Martinioni, D.R. 2001. A review of the geology of the Argentinian
1186 Fuegian Andes. Journal of South American Earth Sciences 14(2): 175-188.
1187 Olivero, E.B.; Medina, F.A.; López Cabrera, M.I. 2009. The stratigraphy of
1188 cretaceous mudstones in the eastern Fuegian Andes: new data from body
1189 and trace fossils. Revista de la Asociación Geológica Argentina 64: 60-69.
1190 Olivero, E.B.; Torres Carbonell, P.J.; Bedoya Agudelo, E.L.; Gutiérrez, C.I.;
1191 Mosqueira González, V. 2025. Estratigrafía del Cretácico Superior-Cenozoico
1192 de las cuencas Austral-Malvinas en los Andes Fueguinos: actualización y
1193 síntesis. Revista de la Asociación Geológica Argentina 82(1): 3-39.

1194 Ortiz, M. 2007. Condiciones de formación del Complejo Metamórfico Cordillera
1195 Darwin, al sur de Seno Almirantazgo, Región de Magallanes, Chile. Tesis
1196 Memoria de Título (Unpublished), Universidad de Chile, Departamento de
1197 Geología: 114 p.
1198 Palotti, P.; Menichetti, M.; Cerredo, M.E.; Tassone, A. 2012. A new U-Pb zircon age
1199 determination for the Lemaire Formation of Fuegian Andes, Tierra del Fuego,
1200 Argentina. Rendiconti Online Della Società Geologica Italiana 22: 170-173.
1201 Passchier, C.W.; Trouw, R.A.J. 2005. Microtectonics. Springer: 366 p. Berlin.
1202 Quensel, P. 1910. Geologisch-petrographische Studien in der patagonischen
1203 Cordillera. Bulletin of the Geological Institution of the University of Upsala 11:
1204 1-114.
1205 Ramos, V.A. 2008. Patagonia: A paleozoic continent adrift? Journal of South
1206 American Earth Sciences 26(3): 235-251.
1207 Riley, T.R.; Burton-Johnson, A.; Flowerdew, M.J.; Poblete, F.; Castillo, P.; Hervé, F.;
1208 Leat, P.T.; Millar, I.L.; Bastias, J.; Whitehouse, M.J. 2023. Palaeozoic-Early
1209 Mesozoic geological history of the Antarctic Peninsula and correlations with
1210 Patagonia: Kinematic reconstructions of the proto-Pacific margin of
1211 Gondwana. Earth-Science Reviews 236: 104265.
1212 Rojas, L.; Mpodozis, C. 2006. Geología estructural de la faja plegada y corrida de
1213 Tierra del Fuego, Andes Patagónicos Chilenos. *In* XI Congreso Geológico
1214 Chileno: 325-328. Antofagasta.
1215 Rossignol, C.; Hallot, E.; Bourquin, S.; Poujol, M.; Jolivet, M.; Pellenard, P.;
1216 Ducassou, C.; Nalpas, T.; Heilbronn, G.; Yu, J.; Dabard, M.-P. 2019. Using
1217 volcaniclastic rocks to constrain sedimentation ages: To what extent are

volcanism and sedimentation synchronous? Sedimentary Geology 381: 46-64.

Sernageomin. 2003. Mapa Geológico de Chile. Servicio Nacional de Geología y Minería. Santiago. 1:1.000.000.

Sharman, G.R.; Malkowski, M.A. 2020. Needles in a haystack: Detrital zircon UPb ages and the maximum depositional age of modern global sediment. Earth-Science Reviews 203: 103109.

Söllner, F.; Miller, H.; Hervé, M. 2000. An Early Cambrian granodiorite age from the pre-Andean basement of Tierra del Fuego (Chile): the missing link between South America and Antarctica? Journal of South American Earth Sciences 13(3): 163-177.

Suárez, M.; Pettigrew, T.H. 1976. An Upper Mesozoic island-arc-back-arc system in the southern Andes and South Georgia. Geological Magazine 113(4): 305-328.

Thomas, C.R. 1949. Manantiales field, Magallanes Province, Chile. AAPG Bulletin 33(9): 1579-1589.

Torres Carbonell, P.J.; Cao, S.J.; Dimieri, L.V. 2017. Spatial and temporal characterization of progressive deformation during orogenic growth: Example from the Fuegian Andes, southern Argentina. Journal of Structural Geology 99: 1-19.

Torres Carbonell, P.J.; Cao, S.J.; González Guillot, M.; Mosqueira González, V.; Dimieri, L.V.; Duval, F.; Scaillet, S. 2020. The Fuegian thrust-fold belt: From arc-continent collision to thrust-related deformation in the southernmost Andes. Journal of South American Earth Sciences 102: 102678.

1242 Twiss, R.; Moores, E. 2007. Structural Geology, 2nd edition. W. H. Freeman and
1243 Co.: 736 p. New York.
1244 Vermeesch, P. 2018. IsoplotR: A free and open toolbox for geochronology.
1245 Geoscience Frontiers 9(5): 1479-1493.
1246 Vermeesch, P. 2021a. On the treatment of discordant detrital zircon U-Pb data.
1247 Geochronology 3(1): 247-257.
1248 Vermeesch, P. 2021b. Maximum depositional age estimation revisited. Geoscience
1249 Frontiers 12(2): 843-850.
1250 Wilson, T.J. 1991. Transition from back-arc to foreland basin development in the
1251 southernmost Andes: Stratigraphic record from the Ultima Esperanza District,
1252 Chile. Geological Society of America Bulletin 103: 98-111.

1253

FIGURE CAPTIONS

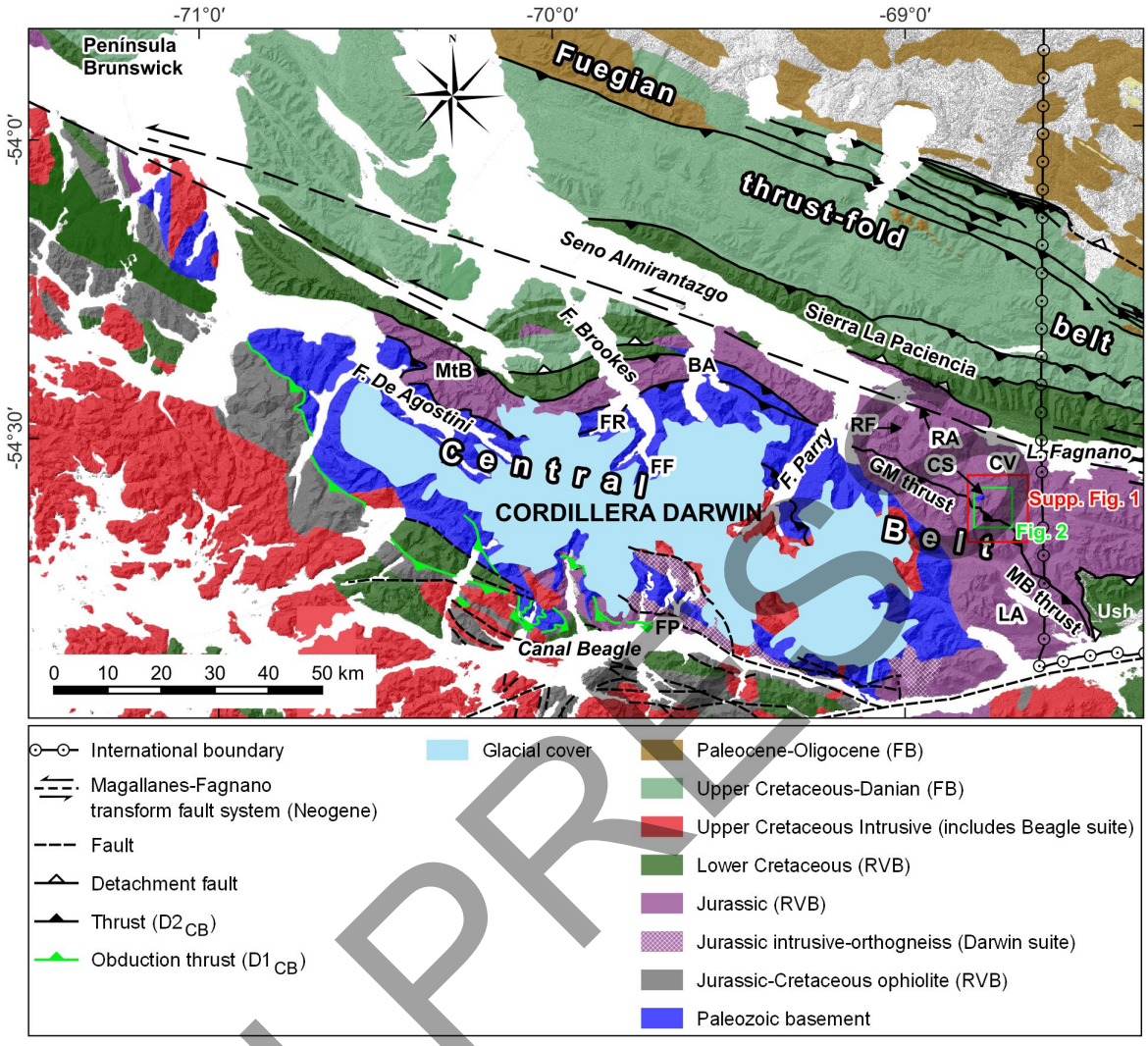

Fig. 1. Geological map of the central belt of the Fuegian Andes focused on Cordillera Darwin. Based on Sernageomin (2003), Hervé et al. (2010a), Klepeis et al. (2010), Cao et al. (2025), and Olivero et al. (2025). FP: Fiordo Pía, CS: Cerro Svea, CV: Cerro Verde, FF: Fiordo Finlandia, GM: Glaciar Marinelli, MB: Mina Beatriz, MtB: Monte Buckland, LA: Lago Acigami, FR: Fiordo Relander, RA: Río Azopardo, RF: Río Fontaine, BA: Bahía Ainsworth, Ush: Ushuaia. FB: Foreland Basin, RVB: Rocas Verdes Basin, $D1_{CB}$ and $D2_{CB}$ explained in text.

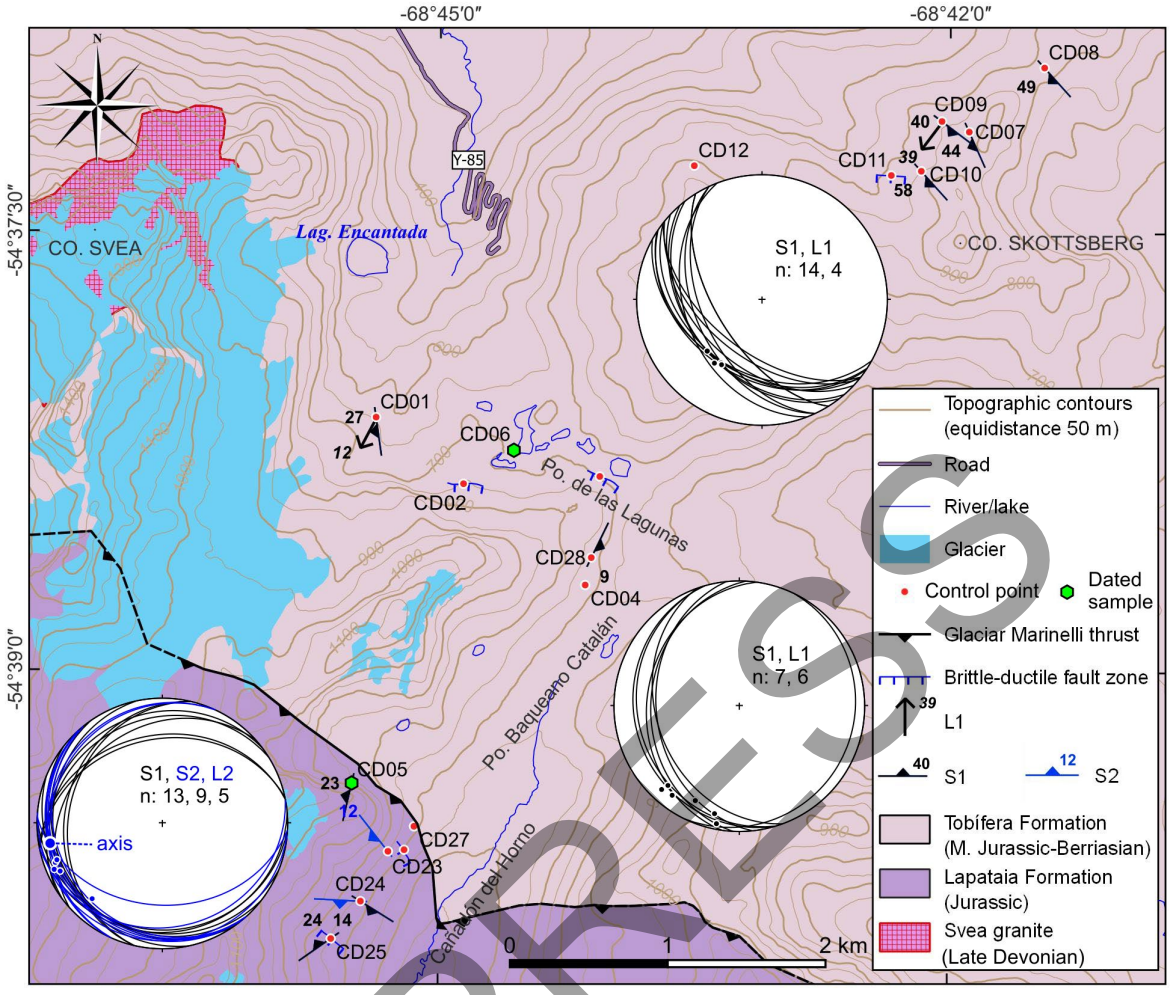

Fig. 2. Geological map of the studied area, with main structural features and stratigraphy based on our results (located in figure 1). Boundaries of the Svea granite are from Mella and Quiroz (2023). Small numbers are dips/inclinations in degrees. The spherical projections are equal-area, lower hemisphere for the areas of Cerro Skottsberg, Paso de las Lagunas, and the hanging wall of the Glaciar Marinelli Thrust. They show planes (great circles) and lineations (small dots) as indicated (black: S1, L1; blue: S2, L2), with n: number of measurements. The axis marked in the Glaciar Marinelli Thrust hanging wall is the theoretical mean folding axis calculated from folded S1 surfaces.

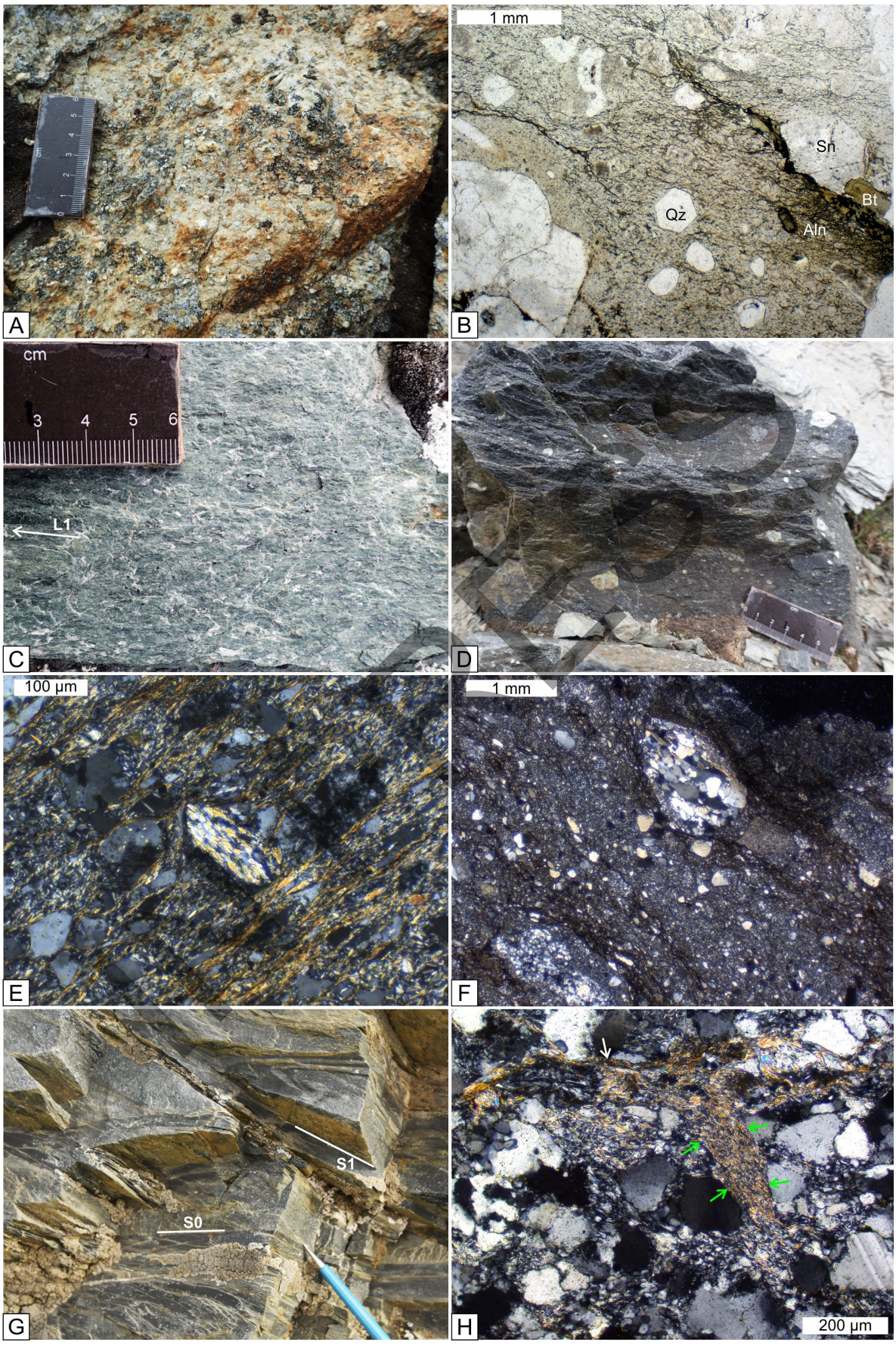

1275

Fig. 3. A. Rhyolite from point CD08, showing porphyritic texture with quartz and feldspar phenocrysts in an aphanitic groundmass. **B.** Photomicrograph (plane-polarized light, PPL) of the same rhyolite with phenocrysts of quartz (Qz), sanidine (Sn) and biotite (Bt). Aln is allanite. Cleavage is NW-SE in the photo (pressure-solution seams). **C.** Chloritic fine-grained schist (CD09) with well-developed cleavage (in plane of photograph) and a stretching lineation (L1) formed by deformed clasts. **D.** Breccia with pebble-sized clasts, mainly of felsic volcanic rocks (CD12). **E.** Photomicrograph (cross-polarized light, CPL) of the breccia shown in D, note foliated clast with an inherited fabric oblique to the NE-SW foliation in the breccia. **F.** Photomicrograph (CPL) of a breccia (CD28) with a clast of foliated metamorphic rock (above center), formed by granoblastic quartz with grain-shape preferred orientation and orientated biotite, contrasting with the disjunctive anastomosed foliation in the breccia matrix. The latter (NW to SE) consists mostly of pressure-solution seams with only very fine metamorphic sericite in the finer fraction. **G.** Metapsammites from CD10, with well-defined layering (S0) and finely spaced cleavage (S1), as well as very tight folds in S0 (upper part of photograph). **H.** Photomicrograph (CPL) of sample CD06, with a foliated metamorphic clast (green arrows). The fine continuous foliation in the clast contrasts with the rough disjunctive foliation in the matrix, which runs horizontally and is marked by pressure-solution seams, flattened and stretched detrital micas (e.g., white arrow) and fine metamorphic sericite.

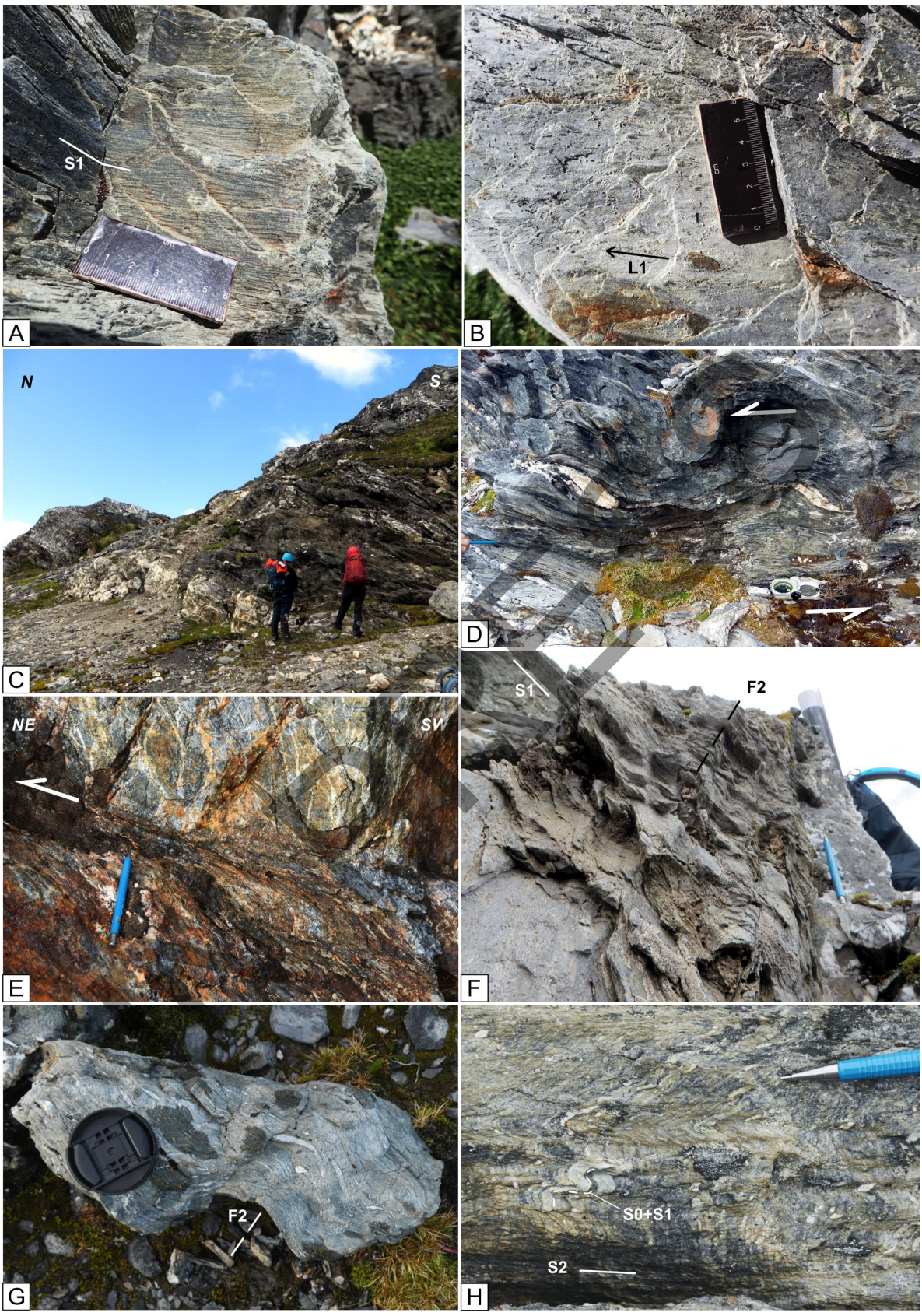

1299

Fig. 4. Structures developed in the footwall of the Glaciar Marinelli Thrust. **A.** S1 foliation in slates intercalated with breccias at point CD01. The transposed stratification remains as dismembered lenses parallel to S1. **B.** L1 stretching lineation in the slates of A, defined by stretched porphyroclasts. **C.** Outcrop example of a brittle-ductile shear zone at CD02. **D.** Detail of the same zone, with deflected S1 surfaces revealing a top-to-northeast shear sense. **E.** Similar fabric at point CD10, where a shear band separates more distributed (ductile) deformation (bottom) from a brittle breccia (top). **F-G.** F2 folds developed on S1 surfaces between points CD04 and CD05 (F), and on breccias near point CD06 (G). Dashed lines indicate F2 axial traces. **H.** Macroscopic relationship between the S2 crenulation cleavage that cross-cuts the transposition foliation formed by parallel S0+S1, in a fine breccia at point CD04.

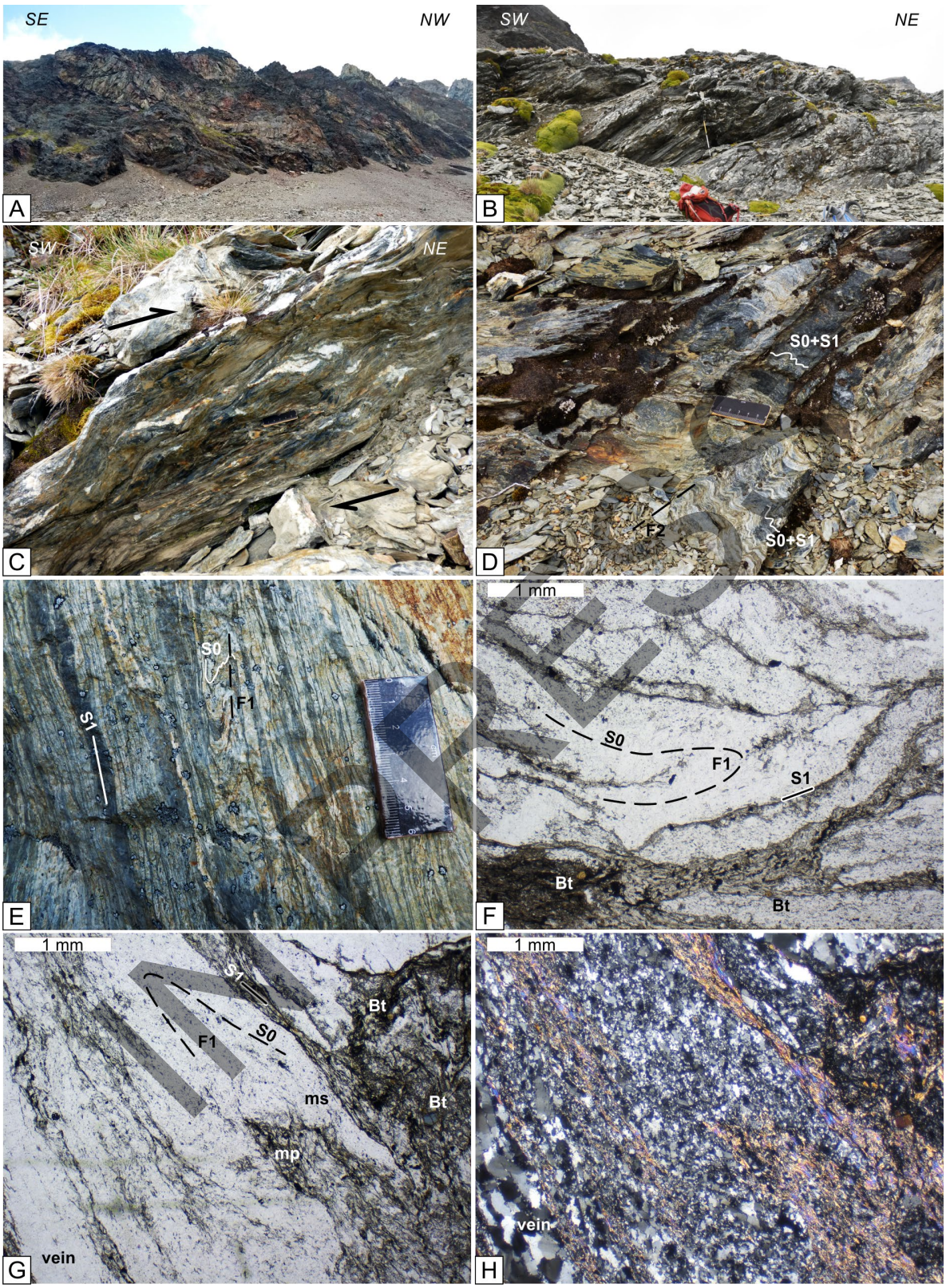

1313

1314 **Fig. 5. A.** Outcrop of the Glaciar Marinelli Thrust at point CD05. The basal part of

1315 the cliff, partly covered by debris, is a 20–30 m thick fault zone. **B.** Outcrop of

the fault zone, from the left end of the escarpment shown in A. **C-D.** Detail of the brittle-ductile fabric, revealing sigmoidal deflection (C) and F2 folds (D) in the transposed sedimentary layering (S0+S1). Photographs from the fault zone shown in B. **E.** Macroscopic view of rootless, isoclinal F1 folds in S0 laminae, and discontinuous S0 bands preserved within the S1 transposition foliation. The dashed black line marks the axial trace of a F1 fold, parallel to S1. Photograph from the footwall directly below the Glaciar Marinelli Thrust. **F-H.** Photomicrographs showing the relationships between S0, the S1 transposition foliation, subparallel veins, and isoclinal F1 folds. mp: metapelite, ms: metapsammite. Notice biotite porphyroblasts (Bt) in the fine micaceous laminae. Detailed descriptions in text. F-G: plane-polarized light, H: same photo as G, cross-polarized light.

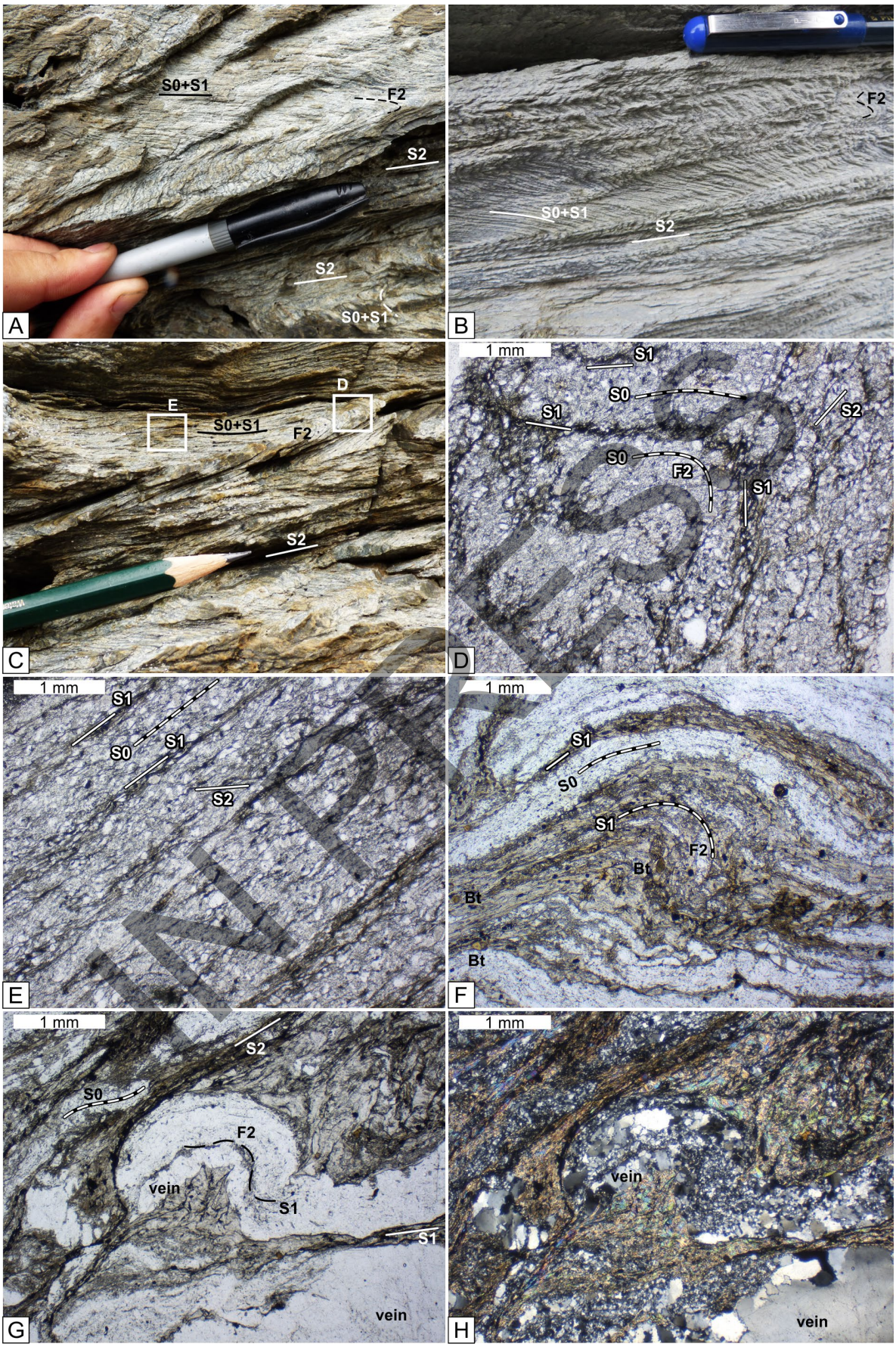
A
S0+S1
F2
S2
S2
S0+S1
B
F2
S0+S1
S2
C
E
S0+S1
F2
D
S2
D
1 mm
S1
S0
S1
S2
S0
F2
S1
E
1 mm
S1
S0
S1
S2
F
1 mm
S1
S0
S1
F2
Bt
Bt
Bt
G
1 mm
S2
S0
F2
vein
S1
S1
vein
H
1 mm
vein
vein

1328

Fig. 6. A-B. Folded S0+S1 bands (S1 transposition foliation with discontinuous subparallel S0 in the microlithons) forming F2 asymmetric folds, axial planar to the S2 crenulation cleavage in the fine schists and phyllites of the Glaciar Marinelli Thrust hanging wall. Notice stronger development of the S2 cleavage at some horizons, where it transposes all prior fabrics into a closely spaced crenulation cleavage. **C.** Similar structure showing equivalent location of photomicrographs D and E (sample CD23), in the hinge zone and limb of an F2 fold. **D-E.** Photomicrographs revealing the relationships between the F2-S2 fabric on prior transposition foliation (S1) and subparallel S0 bands, with better development of S2 in the hinge zones. **F-H.** Photomicrographs revealing folded transposition foliation subparallel to quartz veins, forming F2 folds with axial-planar S2 crenulation cleavage. D-G: plane-polarized light, H: cross-polarized light, same photo as G.

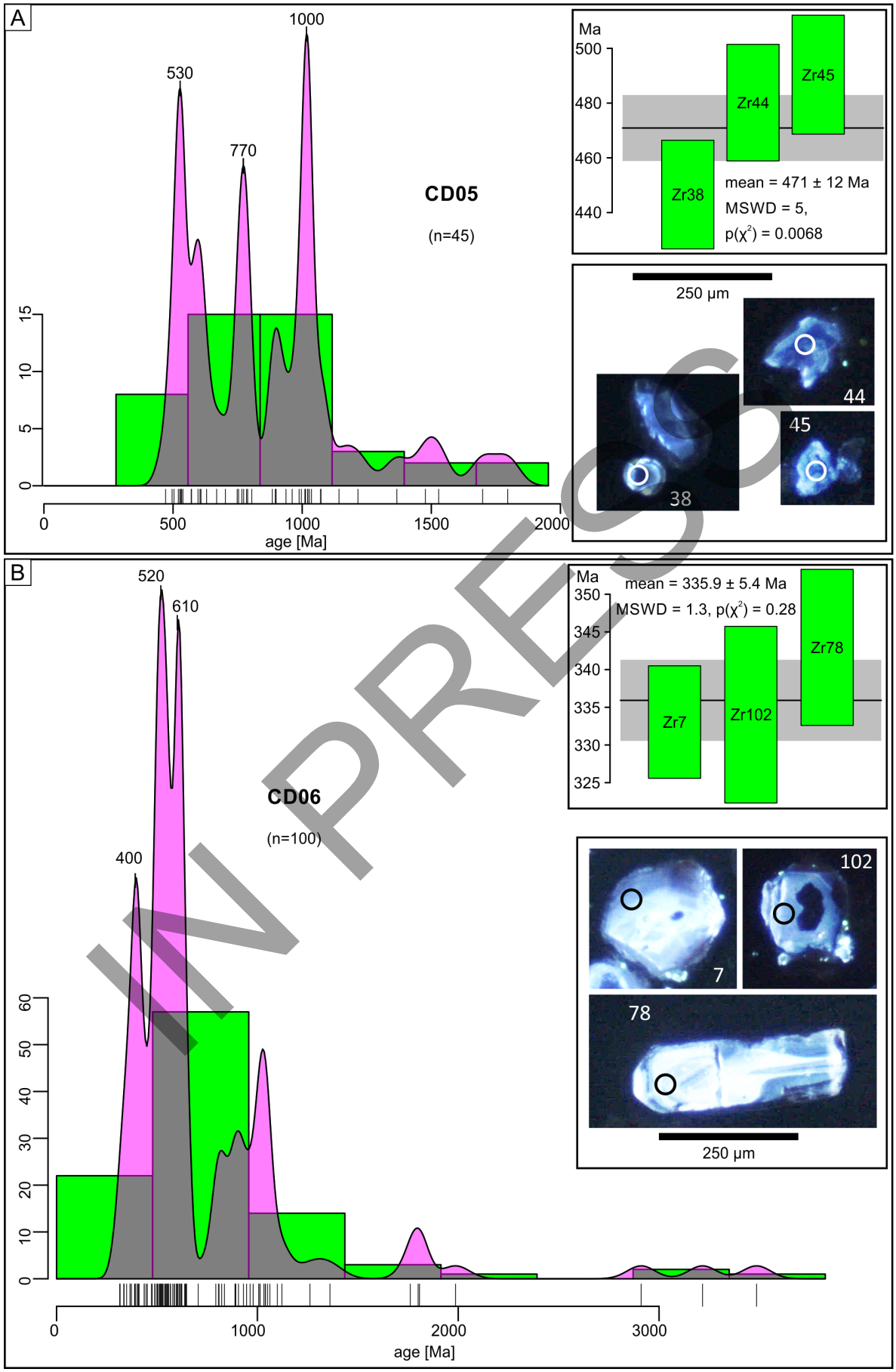

1342

Fig. 7. Geochronological results of samples CD05 (**A**) and CD06 (**B**). KDE diagrams show main Cambrian and Proterozoic peaks. Insets display the Y3Go ages for each sample, with labels indicating the grains used (bar heights are ±2σ). Cathodoluminescence (CL) images of the grains used in the Y3Go age calculations are shown for each sample (see complete CL images in Supplementary Files 5 and 6), notice variable roundness and broken grains. MSWD: mean standard weighted deviation.

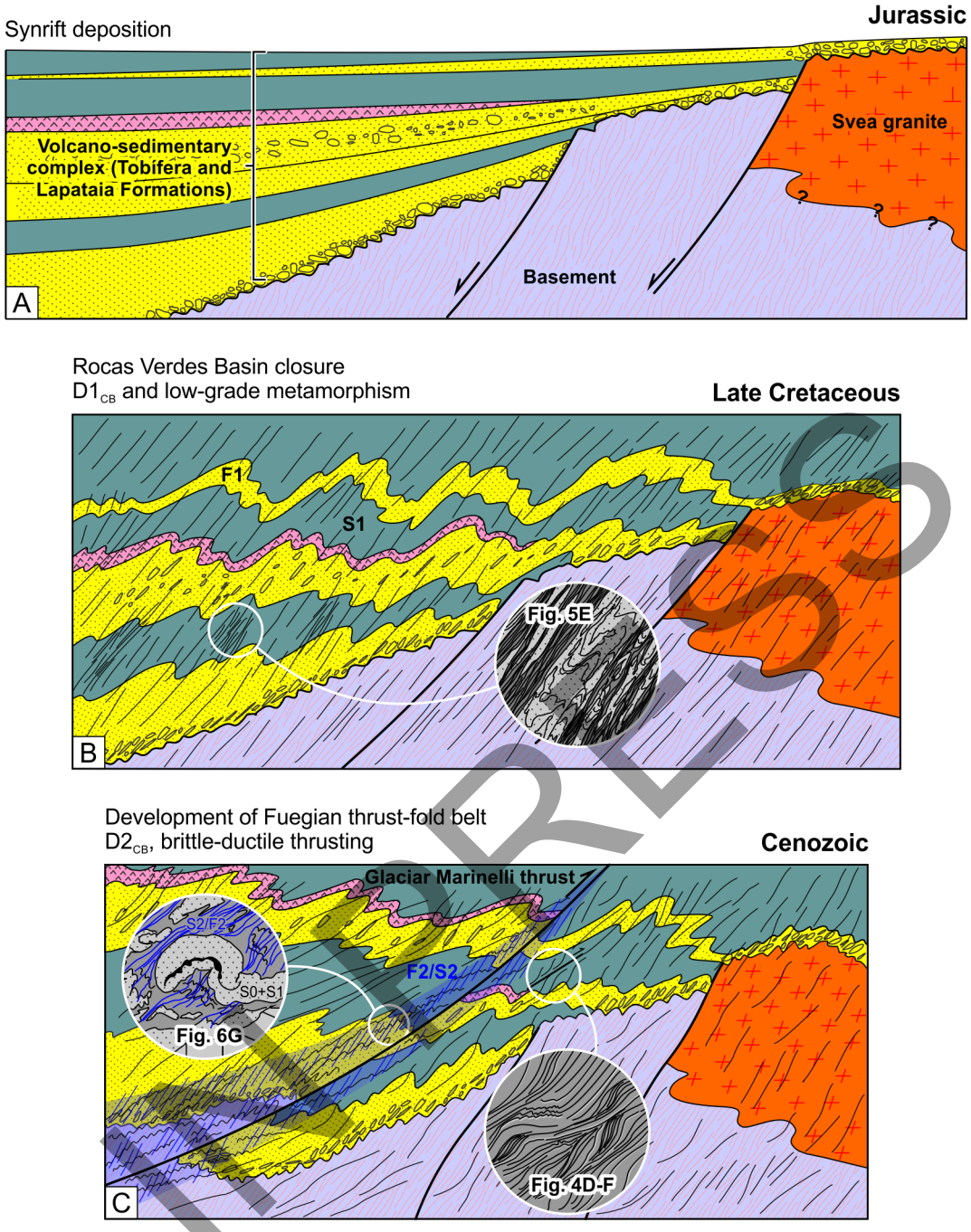

Fig. 8. Cartoon depicting the deformation sequence interpreted from our structural and petrographic data, in the context of the tectonic evolution of the Fuegian Andes. **A.** Jurassic. **B.** Late Cretaceous. **C.** Cenozoic. The extent and cross-cutting relationships of the Svea granite and the normal fault drawn in A, as well as the geometry of the hemigraben, are theoretical and not to scale.

Table 1. Summary of previous stratigraphic work in northern Cordillera Darwin and adjacent areas of the central belt (excluding Lower Cretaceous metasedimentary rocks). See more exhaustive descriptions in the text.

Author(s)	Kranck (1932)	Cortés and Valenzuela (1960)	Nelson *et al.* (1980)	Johnson (1990)	Hervé *et al.* (2010)	Cao *et al.* (2022, 2025)	Mella and Quiroz (2023)
Area/locality	Monte Buckland	Río Fontaine	Northern Cordillera Darwin	Bahía Ainsworth-Fiordo Brookes	Northern Cordillera Darwin	West of Ushuaia	Paso de las Lagunas, Cerro Svea
Unit name *description*	**Monte Buckland Formation** *conglomerates, slates, tuffs*	**Río Fontaine Formation** *conglomerates, sandstones and slates*	*Upper unit: volcaniclastic fine- to coarse-grained rocks*	**Seno Almirantazgo Volcanic-Sedimentary Complex** *volcanic, pyroclastic, sedimentary rock*	**Tobífera Formation (*cf.* Thomas, 1949)** from Permian to Middle Jurassic detrital zircon U-Pb ages	**Lemaire Complex** *volcanic-sedimentary complex Middle Jurassic-Berriasian zircon U-Pb ages*	**Tobífera Formation**
	Quartz-porphiry schists	**Porphyritic Series** *porphyries and slates*	**Cover Complex** *Lower unit: volcanic with basal clastic horizon*	**Basal Clastic Complex** *conglomerates, sandstones, slates*	(Increasing metamorphic grade)	**Lapataia Formation** *metapsamitic quartz-chlorite and quartz-sericite schists and phyllites metabasic greenstones-greenschists*	
	Unconformity		**Unconformity**	**Unconformity**	**Cordillera Darwin Metamorphic Complex** *includes Mesozoic cover and metasedimentites with Cambrian-Devonian detrital zircon U-Pb ages*		*Contact not exposed*
	High Metamorphic Schists or Old Schists *fine micaceous and quartzitic schists*		**Basement complex** *mostly metapelitic*	**Basement** *phyllites and schists (metapsamites) with chlorite, sericite, quartz, albite, calcite, epidote, amphibole, biotite, and garnet (contact metamorphism)*			**Estratos Paso de las Lagunas** *metaconglomerates and quartzites*
							Unconformity
							Cerro Svea granite *Late Devonian muscovite $^{40}Ar/^{39}Ar$ age*

1357

1358

Table 2. Correlation of structural fabrics described in northern Cordillera Darwin (excluding other areas) by previous work and in this study, and their tectonic interpretation. See detailed descriptions in the text.

Tectonic stage	Author and nomenclature		
	Nelson *et al.* (1980)	Klepeis (1994)	This work
Pre-Jurassic deformation in the SW margin of Gondwana	**Db** mostly inferred from deformed-foliated clasts in Jurassic rocks	Hanging wall of the Glaciar Marinelli Thrust: S1, "an early foliation observed mainly in thin section", subparallel to quartz veins	**No pre-Jurassic tectonic fabric**
Late Cretaceous closure of the RVB NE-directed obduction of RVB floor and cover, and SW-directed underthrusting of contiental margin, culminating in arc-continent collision (Bruhn, 1979; Nelson *et al.*, 1980; Cunnigham, 1995; Kohn *et al.*, 1995; Klepeis *et al.*, 2010; Maloney *et al.*, 2011; Betka *et al.*, 2015, 2022). **D1CB deformation in Torres Carbonell *et al.* (2020)**	**D1** In northwest Cordillera Darwin: S1, slaty cleavage axial-planar to open folds L1, associated stretching and intersection lineations	Footwall of Glaciar Marinelli Thrust: S1, "dominant foliation", fine spaced cleavage, cuts sedimentary lamination (S0) L1, downdip mineral lineation on S1 surfaces Hanging wall of the Glaciar Marinelli Thrust: F2, isoclinal folds deforming the S1 early foliation S2, "dominant" foliation, "crenulation cleavage", axial-planar with the F2 folds, coplanar with the footwall S1 L2, downdip stretching lineation on S2	S0 (Jurassic), in the hanging wall of the Glaciar Marinelli Thrust is distinguished as metapsammite (quartz-feldespathic) and metapelite (sericite-chlorite) bands, parallel to quartz veins, and partially transposed by S1 S1, main penetrative foliation in the study area, with stretching lineation L1 Transposed S0 forms intrafolial F1 folds in the more strained zones
Deformation after arc-continent collision with NE-directed thrusting and formation of the Fuegian thrust-fold belt, emplacement of thrust sheets and propagation of deformation to the foreland during the Paleogene to early Neogene. Final exhumation of the central belt (Álvarez Marrón *et al.*, 1993; Klepeis and Austin, 1997; Klepeis *et al.*, 2010; Torres Carbonell *et al.*, 2020; Cao *et al.*, 2023). **D2CB deformation in Torres Carbonell *et al.* (2020)**	**D2** **In northern Cordillera Darwin:** S2, spaced foliation associated with brittle or brittle-ductile structures	Footwall of Glaciar Marinelli Thurst: S2, fine spaced cleavage at low angle to S1 S3, crenulation cleavage that deforms S1 and S2, best development near the Glaciar Marinelli thrust F4, broad and open minor folds, developed on S3 and earlier fabrics Hanging wall of the Glaciar Marinelli Thrust: S3, crenulation foliation, with associated small folds (F3) S3 is deformed by shear bands, with usual top-to-NE shear sense F4, folds in the previous fabrics associated with these shear bands	S2, crenulation foliation best developed near brittle-ductile thrust zones L2, crenulation lineation (intersection of S1 and S2) Associated macroscopic deformation forms F2 folds in close relationship with shear bands

1359

Table 3. Summary of samples from northern Cordillera Darwin dated by Hervé *et al.* (2010a) and discussed in this work.

Sample	Lithology	Unit (*sensu* Hervé et al. , 2010a)	Zircon U-Pb ages
FO0539	Foliated quartzose phyllite from a conglomeratic succession that conformably underlies an ignimbrite bed.	Tobífera Formation (Basal Clastic Complex)	Dominant Carboniferous peaks (*ca.* 340–360 Ma), and older peaks and scattered ages. Two grains record Jurassic dates (3 spots, one from SHRIMP). Dominated by Early Devonian peak (404±5 Ma). Pre-Devonian ages between 600–680 Ma.
FO0508	Quartz-rich amphibole-bearing foliated rock.	Cordillera Darwin Metamorphic Complex (interpreted Tobífera Formation Basal Clastic Complex)	9 spots in 6 grains of Jurassic age, eight form a peak around 166±2 Ma. these ages come from grains that are predominantly igneous in origin.
FO0516	Granitic clast from a matrix-supported foliated conglomerate.	Tobífera Formation (Basal Clastic Complex)	Single population of zoned igneous zircon, 18 grains give a weighted mean age of 466±3 Ma (Ordovician).
FO0524	Feldspathic litharenite, with quartz, plagioclase, slate or phyllite, quartzite and marble clasts. Foliated metamorphic rock fragments comprise 25% of the sample (Ortiz, 2007). It is part of a succession in which clast-supported conglomerates containing 1–10 cm pebbles of quartz, micaschist and volcanic rocks predominate.	Tobífera Formation (Basal Clastic Complex)	Predominant broad Cambrian peak (ca. 530–550 Ma). Youngest peaks of Permian and Triassic ages at ca. 270 and 245 Ma. Scattered older ages.

1360